Insight into Insulin Secretion from Transcriptome and Genetic Analysis of Insulin-Producing Cells of *Drosophila*

Jian Cao,* Julie Ni,*,[1] Wenxiu Ma,*,[2] Vanessa Shiu,* Luis A. Milla,* Sangbin Park,* Maria L. Spletter,[†] Sheng Tang,* Jun Zhang,* Xing Wei,[†] Seung K. Kim,*,[‡] and Matthew P. Scott*,[‡,§,,3]**

*Departments of Developmental Biology, [§]Genetics, [**]Bioengineering, [†]Biology, and [‡]Howard Hughes Medical Institute, Stanford University School of Medicine, Stanford, California 94305

ABSTRACT Insulin-producing cells (IPCs) in the *Drosophila* brain produce and release insulin-like peptides (ILPs) to the hemolymph. ILPs are crucial for growth and regulation of metabolic activity in flies, functions analogous to those of mammalian insulin and insulin-like growth factors (IGFs). To identify components functioning in IPCs to control ILP production, we employed genomic and candidate gene approaches. We used laser microdissection and messenger RNA sequencing to characterize the transcriptome of larval IPCs. IPCs highly express many genes homologous to genes active in insulin-producing β-cells of the mammalian pancreas. The genes in common encode ILPs and proteins that control insulin metabolism, storage, secretion, β-cell proliferation, and some not previously linked to insulin production or β-cell function. Among these novelties is *unc-104*, a kinesin 3 family gene, which is more highly expressed in IPCs compared to most other neurons. Knockdown of *unc-104* in IPCs impaired ILP secretion and reduced peripheral insulin signaling. Unc-104 appears to transport ILPs along axons. As a complementary approach, we tested dominant-negative Rab genes to find Rab proteins required in IPCs for ILP production or secretion. Rab1 was identified as crucial for ILP trafficking in IPCs. Inhibition of Rab1 in IPCs increased circulating sugar levels, delayed development, and lowered weight and body size. Immunofluorescence labeling of Rab1 showed its tight association with ILP2 in the Golgi of IPCs. Unc-104 and Rab1 join other proteins required for ILP transport in IPCs.

SIGNALING through the evolutionarily conserved insulin pathway is critical for organismal homeostasis, controlling everything from growth regulation and development to metabolic homeostasis through glucose and lipid metabolism. In mammals, insulin synthesis and release takes place in pancreatic β-cells. Insulin production is regulated by many factors such as nutrient status and hormonal signals (Newsholme *et al.* 2010). After translation, insulin is packaged into dense-core vesicles (DCVs) and trafficked to the plasma membrane. Transport of insulin-containing DCVs is microtubule dependent, and the microtubule motor kinesin-1 is known to influence insulin granule transport (Meng *et al.* 1997; Tabei *et al.* 2013). DCV transport is additionally regulated by Rab27a. Through its effectors Slac2c, Noc2, Slp4, Exophilin8, and coronin3, Rab27a regulates movement of DCVs and their docking and fusion to the plasma membrane (Yi *et al.* 2002; Kasai *et al.* 2005; Kimura *et al.* 2008; Kimura and Niki 2011; Wang *et al.* 2013). DCV release is modulated largely via glucose stimulation and internalization, resulting in increased β-cell ATP levels. This induces the closure of ATP-dependent potassium channels and cell depolarization, triggering an influx of calcium ions through voltage-dependent calcium channels. Ca^{2+} promotes formation of the SNARE complex, allowing DCV fusion and insulin release (Kasai *et al.* 2010). Thus, proper packaging, trafficking, and exocytosis of insulin-containing DCVs is central to regulating insulin secretion. Defects in insulin production and trafficking arise early in the pathogenesis of diabetes. Many factors involved in DCV trafficking and the molecular details of DCV release remain elusive.

Research in animal models, in particular in *Drosophila* with its large genetic toolkit and fast generation time, can

doi: 10.1534/genetics.113.160663
Manuscript received December 12, 2013; accepted for publication February 10, 2014; published Early Online February 20, 2014.
Available freely online through the author-supported open access option.
Supporting information is available online at http://www.genetics.org/lookup/suppl/doi:10.1534/genetics.113.160663/-/DC1.
[1]Present address: A125 Nelson Labs, Molecular Biology and Biochemistry Department, Rutgers University, Piscataway, New Jersey 08854.
[2]Present address: Department of Genome Sciences, University of Washington, Seattle, WA 98195.
[3]Corresponding author: Clark Center, 318 Campus Dr., Stanford University School of Medicine, Stanford, CA 94305. E-mail: mscott@stanford.edu

provide mechanistic insights into insulin-like peptide (ILP) production and DCV transport and release. *Drosophila* ILPs are homologous to human and mouse insulin/insulin-like growth factors (Brogiolo *et al.* 2001). Deletion of *Ilps 1-5* results in smaller flies with lower metabolic activity (Zhang *et al.* 2009), while ubiquitous overexpression of *Ilp2* is sufficient to promote growth (Ikeya *et al.* 2002). In flies, ILPs are produced and secreted mainly by insulin-producing cells (IPCs) in the brain to control growth and metabolism (Ikeya *et al.* 2002; Rulifson *et al.* 2002). ILP secretion is dependent on autonomous regulation and on inputs received from other cellular populations (Colombani *et al.* 2003; Geminard *et al.* 2009; Bai *et al.* 2012; Rajan and Perrimon 2012). ILPs are also produced by fat body cells during the pupal nonfeeding stages (Okamoto *et al.* 2009; Slaidina *et al.* 2009). Flies that lack IPCs have delayed development, reduced growth, and increased circulating sugar levels (Rulifson *et al.* 2002), suggesting that IPCs in flies play a role comparable to β-cells in mammals.

IPCs number only 14 of ~100,000 neurons. They develop from a single pair of neuroblasts in the anterior neuroectoderm during late embryogenesis (Wang *et al.* 2007). During larval stages, IPCs secrete ILPs to promote growth and regulate sugar metabolism, while concurrently undergoing morphological development. Although the morphological development of IPCs during larval stages has not been well characterized, their neuronal processes extend through the brain to the aorta and the corpora cardiac compartment of the ring gland for ILP release (Rulifson *et al.* 2002). Adult IPCs are important for regulating starvation resistance, responding to oxidative and temperature stress, and adjusting carbohydrate and lipid metabolism (Nassel 2012).

The long neurites of larval and adult IPCs suggest that ILPs require extensive intracellular transport to reach secretion sites, the mechanism of which is largely unexplored. To identify additional cellular components that are important for insulin secretion *in vivo*, we sequenced messenger RNA (mRNA) purified from IPCs and identified IPC-enriched gene expression. To obtain a relatively pure population of fly IPCs for mRNA extraction, we used laser-capture microdissection (LCM). Compared with other cell- and tissue-specific RNA isolation techniques for *Drosophila*, including FACS (Tirouvanziam *et al.* 2004), magnetic bead-based cell purification (Iyer *et al.* 2009), and RNA-binding protein-based strategies (Miller *et al.* 2009), LCM has advantages for isolating specific cell types, especially for cells that are clustered, like IPCs. LCM has a reasonably high degree of spatial resolution and accuracy (Iyer and Cox 2010). We first characterized the temporal development of IPCs in detail and analyzed the transcriptome of early third instar IPCs. We identified 193 genes as enriched in IPCs, in comparison to randomly captured neurons, and found that many orthologous genes are active in mammalian pancreatic β-cells. In parallel, we tested 31 YFP-tagged dominant-negative (DN) Rab proteins (Zhang *et al.* 2007) for genes involved in ILP transport. Rab proteins, members of the family of Ras-like GTPases, control many cellular trafficking paths (Stenmark 2009). Our two approaches identified two genes essential in *Drosophila* for proper trafficking and secretion of ILP-containing DCVs. Here we identify Rab1 as necessary in IPCs to modulate ILP secretion. We discovered a novel function for Unc-104/Kif1a, a kinesin-3 microtubule motor previously known to transport synaptic vesicles (Okada *et al.* 1995; Pack-Chung *et al.* 2007; Barkus *et al.* 2008), in the transport of DCVs along the axons of IPCs.

Materials and Methods

Fly strains and genetics

Fly lines used are listed in Supporting Information, Table S6. The temperature shift for Gal80^{ts} experiments was conducted in the following way: Embryos were collected on a molasses cap within a 4-hr period at 25° followed by 40-hr incubation at 18°. Thirty newly hatched first instar larvae were then transferred to each vial, kept at 18° for another 4 days, and shifted to 29° for 24 hr before dissection. Fly food (2×: 3.4% yeast, 8.3% cornmeal, 6% sucrose, 1% agar) was used to raise flies (Geminard *et al.* 2009).

Laser microdissection

The method was adapted from Spletter *et al.* (2007). Early third instar larval brains were dissected and quickly aligned and frozen with optimal cutting temperature compound (Tissue Tek). We sectioned from the posterior end of the mouth hook to the posterior end of the brain lobes, the position of which was marked by the anterior end of a pupa at one end of the block. A dehydration series (distilled H_2O for 1 min, 50% ethanol for 30 sec, 70% ethanol for 30 sec, 95% ethanol for 30 sec, 100% ethanol for 30 sec, 100% ethanol for 2 min, xylene for 2 min, xylene for 5 min) was conducted before each section (10 μm thick) was examined under fluorescence with a 20× objective to identify sections that contain IPCs. IPCs were marked by expression of a genetically encoded GFP reporter (an *Ilp2-Gal4* driving a *UAS-mCD8-GFP* reporter gene). In addition, *UAS-nuclear red fluorescent protein* (RFP) was included in the same fly line to independently label IPC cell bodies with RFP. This double labeling of IPCs, together with strong expression of mCD8-GFP (two copies) in these neurons, significantly sped up the process and reliability of IPC identification in cryosections. IPC-enriched samples were captured into PCR tube caps on a Leica LCM microscope (model ASLMD) using Laser Microdissection software version 4.4.

RNA isolation, amplification, and mRNA sequencing library construction

Total RNA of laser-captured samples was extracted using Arcturus PicoPure RNA Isolation Kit (Molecular Devices). mRNA was amplified in two rounds using the Arcturus RiboAmp HS PLUS Amplication Kit (Molecular Devices). Amplified mRNA from each sample was fragmented to

100–200 nt using 10× RNA fragmentation buffer (Ambion). Fragmented RNAs were ligated to the 3′ linker ("Linker-1," IDT Inc.) and 5′ linker [5′-ACGCTCTTCCGATCTv-3′ (uppercase, DNA; v, barcodes with four RNA molecules: cugg, cguc, acuu, or cccu (IDT Inc.)]. Complementary DNA (cDNA) was amplified with 18 PCR cycles, using forward primer 5′-GAT ACG GCG ACC ACC GAG ATC TAC ACT CTT TCC CTA CAC GAC GCT CTT CCG ATC T-3′ and reverse primer 5′-CAA GCA GAA GAC GGC ATA CGA GCT CTT CCG ATC TAT TGA TGG TGC CTA CAG-3′ to produce sequencing libraries for the Illumina GA II sequencing system. The details of the RNA library construction protocol are available in File S5.

For whole brain (*Elav-Gal4* > w^{1118}), total RNA from third instar larval brains was extracted using Trizol (Invitrogen) following the manufacturer's instructions. No mRNA amplification was used. mRNA sequencing libraries were constructed using a TruSeq RNA sample preparation kit (Illumina).

Mapping sequencing reads and mRNA profiling

Barcode splitting was performed on the FASTQ file. The first four bases of each read were compared to the barcodes, and up to one mismatch was allowed in the barcode bases. After barcode splitting and read segregation, each mRNA sample was aligned using tophat (version 2.0.0) (Trapnell *et al.* 2009), with default parameters against the reference *Drosophila melanogaster* genome and transcriptome [dm3/BDGP Release 5, from the University of California at Santa Cruz (UCSC) Genome Browser] (Adams *et al.* 2000; Fujita *et al.* 2011). Next, cuffdiff in the cufflinks package was used to determine differentially expressed genes and transcripts between the IPC replicates and the control replicates (Trapnell *et al.* 2010), where Reads Per Kilobase of exon model per Million mapped reads (RPKM) was calculated for each gene/transcript in each cell type and compared with each other.

Database for Annotation, Visualization and Integrated Discovery functional annotation analysis

Functional annotation of 193 IPC-enriched transcripts was carried out using the Database for Annotation, Visualization and Integrated Discovery (DAVID) v6.7 (Huang da *et al.* 2009a,b). Entrez_IDs of the 193 genes were used as input. A total of 191 of 193 Entrez_IDs were annotated as known *Drosophila* genes by DAVID. Among the 191 known *Drosophila* genes, 115 (60.2%) genes have biological function annotations in the GOTERM_BP_FAT database. Annotation categories were searched and clustered using GOTERM_BP_FAT databases. Biological functional clusters were ranked based on an enrichment score, which was statistically measured by Fisher's exact test in DAVID.

Searching mouse homologs of fly genes

Mouse homologs of IPC-enriched genes were found in the National Center for Biotechnology Information (NCBI) HomoloGene Database Release 66 (http://www.ncbi.nlm.nih.gov/homologene/). This method identified mouse orthologs of 104 IPC-enriched genes (193 in total). In addition, five homolog pairs (*Ilp2-Ins1*, *Ilp3-Ins1*, *Ilp5-Ins2*, *ia2-IA2*, *foxo-Foxo1*) were added based on literature information (Brogiolo *et al.* 2001) and a BLAT (UCSC genome browser) homologous sequence search.

Fly tissue fixation and immunofluorescence

Fly brains or fat bodies were dissected in ice-cold PBS containing 0.1% Triton X-100 (PBST), and tissues (brains or fat bodies) were fixed in 4% paraformaldehyde for 20 min, followed by extensive washes with PBST. Five-percent normal goat serum (NGS) (Sigma, diluted in PBST) was added to fixed samples for 1 hr at room temperature for blocking. Subsequently, after washing out the NGS, primary antibodies [rat anti-ILP2 (Pierre Leopold); chick anti-GFP (Aves Labs); rabbit anti-mCherry/mtdTomato/dsRed (Clontech); rabbit anti-β-galactosidase (MP Biomedicals)] were diluted in 5% NGS and incubated with the samples at 4° overnight. After extensive washes with PBST, secondary antibodies (anti-rat Alexa 488, anti-rat Alexa633, anti-chick Alexa 488, and anti-rabbit Alexa 647) (Invitrogen) were diluted in 5% NGS and incubated with samples at 4° overnight. After PBST washes, samples were mounted in SlowFade Gold antifade reagent (Invitrogen) for slide preparation.

Fly weighing and pupae volume measurement

Embryos were collected on a molasses cap within a 4-hr period followed by a 24-hr incubation at 25°. Thirty newly hatched first instar larvae were then transferred to each vial and stayed at 29° until eclosion. Adult males (1–2 days after eclosion) from each vial (typically in groups of 10–20) were weighed on an analytic balance accurate to ±0.01 mg (Mettler Toledo). In the cases where balancer exists for the UAS-RNA interference (RNAi) lines or few adults emerged from each vial, males from multiple vials were combined for weighing.

Pupae were photographed. Pupae length (L) and diameter (D) were measured using ImageJ. *Drosophila* pupae are assumed to take the shape of an ellipsoid, and their volume could be estimated based on this shape. Pupae volume (V) was calculated using the following formula: $V = (4/3) \times 3.14159 \times (D/2)^2 \times (L/2)$.

Trehalose and glucose measurement

Trehalose assay was performed as previously described (Rulifson *et al.* 2002). In brief, hemolymph—circulatory fluid in arthropods—from five to eight larvae was collected by tearing the cuticles and allowing the hemolymph to bleed out and pool on a siliconized glass slide. Hemolymph samples (0.5 μl) as well as trehalose and glucose standards were diluted in 100 μl of Infinity Glucose Reagent (Sigma), and 40 μl of the diluted hemolymph was mixed with 80 μl of Infinity Glucose Reagent with porcine trehalase added at

3 μl/ml in 96-well plates. After a 16- to 18-hr incubation at 37°, plates were read on a fluorescence plate reader (Bio-Tek Instruments model #FL600). Excitation was applied at 360 nm while emission occurred at 460 nm. Standard curves were generated for determining the combined glucose and trehalose concentration in hemolymph samples.

Quantitative RT-PCR

For each genotype, 3 × 10 third instar larval brains were collected and RNA was purified using RNAsy kit (Qiagen) according to the manufacturer's instructions. RNA concentration was measured using a NanoDrop 2000 spectrophotometer (Thermo Scientific). cDNA was synthesized from 1 μg RNA using a high-capacity cDNA reverse transcription kit (Applied Biosystems). Quantitative PCR (qPCR) reactions for each biological sample were carried out in duplicate using Taqman assays (Applied Biosystems) for *Ilp2* and *Rpl32*. mRNA levels were compared between conditions using the ΔΔCt method.

Confocal microscopy and image quantifications

Fly and pupae images were captured using a Leica MZ FLIII fluorescenct dissecting microscope and a Leica DFC 500 camera. Images were acquired using a TCS SP2 confocal microscope (Leica) with a ×63/numerical aperture 1.4 oil-immersion objective. To quantify ILP2 levels, confocal Z-series of the IPCs were obtained at 1 μm step size with identical laser power and scanning settings between control and experimental samples. Image stacks were then projected into a Z-stack (sum intensity), and the mean fluorescence intensities across IPC cell bodies or fat body nuclei were measured using Image J (National Institutes of Health). For each larva, multiple brain IPCs were quantified and averaged. These averaged values were then used for statistics to estimate the variance between animals under the same genetic background. Error bars represent the standard error of the mean from at least three independent experiments.

Statistics

For fly weighing, pupae volume, trehalose level, IPC cell number, ILP fluorescence intensity, and qPCR results, data were represented as mean ± SEM. Student's *t*-tests (two tailed, equal variance) were performed for statistical significance.

Results

IPC morphological changes during development

In preparation for laser dissection, we examined the developmental steps in the formation of IPCs to determine optimal conditions and timing for the dissection. Specification of fly brain IPCs during late embryogenesis has been characterized by several studies (Wang *et al.* 2007; Miguel-Aliaga *et al.* 2008; Hwang and Rulifson 2011), while post-specification developmental events such as neuronal morphogenesis of IPCs have been little studied. We followed the development of IPC morphology using *Ilp2-Gal4*-driven membrane (CD8) GFP (Figure 1 and File S1, File S2, File S3, and File S4). At early larval stages, IPCs exist as two symmetrical groups consisting of seven cells in each of the brain hemispheres. Their neuronal processes extend laterally and posteriorly within the brains, with some ending outside the brain, potentially on the aorta and the corpora cardiac compartment of the ring gland (Rulifson *et al.* 2002) (Figure 1 and File S2). At later larval stages, the cell bodies increase in size and their projections extend over greater distances. During pupal stages, the processes that had extended laterally from IPCs during larval stages are gradually dismantled. The processes that initially extended posteriorly from IPCs lengthen and eventually converge into one bundle (Figure 1 and File S3). At later pupal stages, the two IPC clusters converge to form one cell group near the midline. During adulthood new processes beneath IPCs are formed. These extend laterally with extensive arborizations. The posterior projection bundle becomes thickened, with extensive arborization at the terminals (Figure 1 and File S4). Larval IPCs are necessary for growth control and sugar homeostasis (Rulifson *et al.* 2002; Haselton and Fridell 2010). The adult IPCs, like larval IPCs, project to the corpora cardiac and to the aorta for ILP release (Rulifson *et al.* 2002; Kim and Rulifson 2004; Tatar 2004).

In the third instar, IPCs are clustered in two symmetrically organized groups of seven neurons (Figure 2A). The neurons' structural characteristics and arrangement at this stage make them convenient for identification and laser capture. We chose early third instar larvae as the IPC source for two reasons: (1) the rapid growth during second and third instars is indicative of the need for IPC-secreted ILPs. (2) Neurite structures of IPCs do not change much during the third instar (Figure 1), making it more likely that active genes contribute to IPC-regulated ILP production rather than IPC neurite development.

Amplifying sequences of mRNAs extracted from laser-captured larval IPCs

Frozen brain sections containing IPC cell bodies were identified using *Ilp2-Gal4 > mCD8-GFP* and *Ilp2-Gal4 > nuclearRFP*. During larval stages, the Ilp2-Gal4 driver is expressed at low levels in imaginal discs and at high levels in salivary glands and the 14 brain IPCs. In the brain, expression of the Ilp2-Gal4 drive is not detectable outside IPCs (Brogiolo *et al.* 2001; Rulifson *et al.* 2002). The successful capture of IPCs was demonstrated by the absence of GFP-labeled tissue from the residual sections (Figure 2, B and C). In total, 46 IPC cell bodies from 10 brains were captured and equally divided into two groups (IPC1 and IPC2). Two samples (control 1 and control 2) of ~100 non-IPC, non-GFP cells each were collected from the same sections from which IPCs were captured. These adjacent regions of the brain are enriched in neurons that form the superior lateral, superior medial, and ventrolateral protocerebrum, dorsolateral neurons, mushroom body, optic tubercle, and lateral horn.

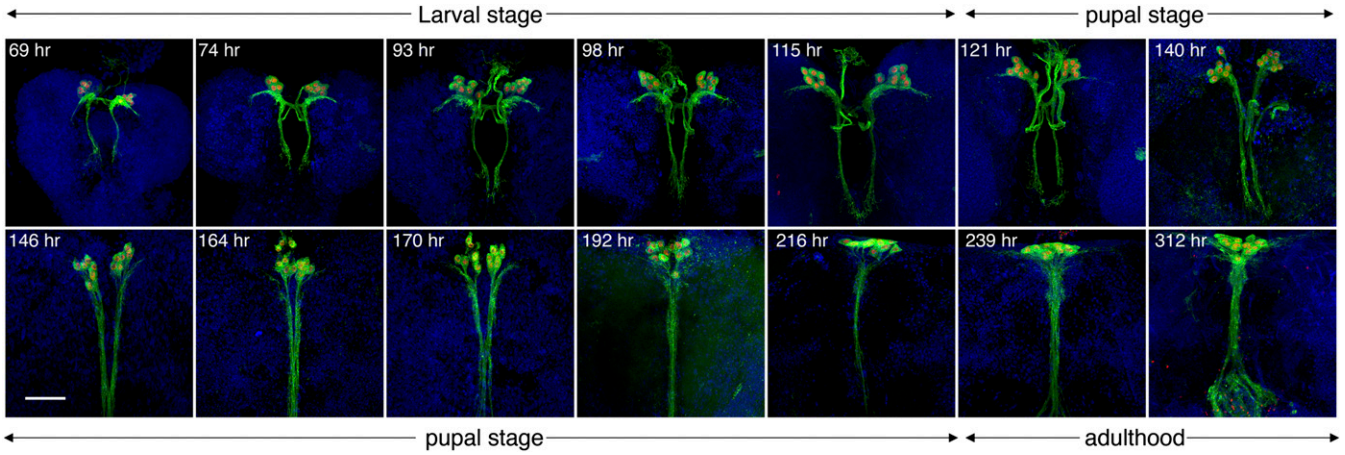

Figure 1 IPC morphology changes during development. IPC neuronal structures were followed from early larval to adult stages. Developmental time points after embryo deposition are indicated. Green: *Ilp2 > mCD8-GFP*; red: *Ilp2 > nuclear-RFP*; blue: DAPI. up: anterior; down: posterior. Shown are maximum z-projections of confocal images taken at 1-μm step size. Flies were raised at 25° throughout development. Bar, 50 μm.

The small amount of RNA isolated from laser-captured cells necessitated amplification of the RNA sequences while trying to minimally skew relative mRNA abundances. We performed two rounds of RNA amplification from each of the four initial samples. In each round of RNA amplification, poly(A)RNA was reversed-transcribed to cDNA, which was then used as template for T7-based *in vitro* transcription to produce amplified RNA (Wang 2005). One limitation of this RNA amplification method is the lower 5′ representation of amplified RNA due to inefficient reverse transcription at each round of the amplification step (Baugh *et al.* 2001; Wang 2005) (Figure 3A). Two rounds of amplification may be insufficient for amplifying the low-copy-number mRNA species. Despite these potential problems, this amplification strategy produces a high correlation of gene expression profiles between unamplified RNA and RNA amplified from low-input RNA (500 pg of total RNA) (Van Gelder *et al.* 1990; Wang *et al.* 2000; Baugh *et al.* 2001; Lang *et al.* 2009). To evaluate the fidelity of the LCM and RNA amplification, we used RT-PCR to verify that the major larval Ilp mRNAs were enriched in amplified samples from captured IPCs, not in laser-dissected control samples (Figure 3B).

After aligning the sequencing reads to the reference *D. melanogaster* genome and transcriptome (dm3/BDGP Release 5 from UCSC genome browser, Table S1; *Materials and Methods*) (Adams *et al.* 2000; Fujita *et al.* 2011), we deduced the presence of transcripts representing 1851 genes that were common to both IPC samples and 2941 genes that were common to both control samples (RPKM ≥ 5.0 for moderate-to-high gene expression level) (Figure 3, C and D; Table S2). The number of expressed genes (total of 3373 from IPC and control samples) is 56% fewer than the number of genes detectably represented in third instar larval whole-brain mRNA-seq data (7704 genes, or 55% of the total fly genes). The lower transcriptome representation of our laser-dissected samples may be due to (1) the mRNAs from the 46 captured IPC cells and the ~200 captured cells presumably from a subset of the genes that are expressed in the whole brain and (2) RNA degradation during LCM and/or insufficient mRNA amplification during IPC and control sample preparation.

Comparing IPCs to the control samples from adjacent regions, 1419 genes are expressed in both. A total of 432 genes are expressed only in IPC samples (IPC1 and IPC2), and 1522 genes are expressed only in control samples (control 1 and control 2). Among the 1419 shared genes, the majority showed little variance in gene expression level between IPCs and controls; most of them are clustered around the diagonal (Figure 3C; see also Table S2).

To select mRNAs that are more abundant in IPCs compared to control cells, we used the following criteria: (1) moderate-to-high expression level in IPCs (RPKM ≥5.0 in both IPC samples); (2) higher expression in IPCs than in controls for both replicates (both $RPKM_{IPC1}$ and $RPKM_{IPC2}$ must be greater than $RPKM_{Control1}$ and $RPKM_{Control2}$); (3) at least twofold enrichment of expression in IPCs compared to controls ($RPKM_{IPC(average)}/RPKM_{Control(average)} \geq 2.0$); and (4) a statistically significant difference between expression in IPCs and expression in controls (P-value ≤ 0.15 by cuffdiff software).

In total, we detected 193 genes that were significantly enriched in IPCs compared to controls (Table S3). To identify the biological function groups represented by the IPC-enriched transcripts, we used DAVID, a gene functional classification tool (http://david.abcc.ncifcrf.gov). Genes were grouped into clusters based upon their gene ontology terms (GO terms) to identify genes sharing common biological functions (Table 1 and Table S4). Among the IPC-enriched transcripts analyzed by DAVID, the most enriched biological process cluster contains genes encoding the ILPs, G-protein-coupled receptors responding to hormone stimulation (*Dh31-R*, *CCHa2-R*, and *mAChR*), and other signaling transducers

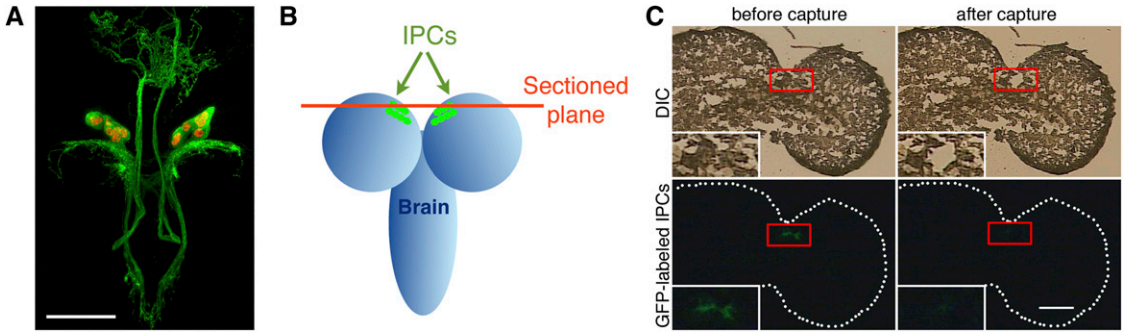

Figure 2 Capture of IPCs through laser microdissection. (A) *Drosophila* IPCs viewed by confocal microscopy. Green depicts IPC neuronal processes and cell bodies, and IPC cell nuclei are in red. (B) Schematic describing the cryosections that were chosen for IPC laser capture. (C) GFP-labeled IPCs before and after laser capture. Red boxes outline where IPCs are located and insets show higher magnifications of those regions. Dotted lines demarcate the boundary of the brain. Bars, 50 μm.

(*Ggamma30A*, *Ras85D*, *Hrs*, and *drl*). Genes in this group are essential for ILP production and could be required for IPCs to sense and process upstream neuronal/hormonal signals that act on IPCs. *chico* and *foxo*, both functioning in the ILP-receiving cells (Bohni *et al.* 1999; Puig *et al.* 2003), were enriched in IPCs, suggesting a possible autocrine role for ILPs to feed back to IPCs. The second most enriched biological process cluster contains genes encoding sugar metabolic enzymes: *Pfk*, *Mdh2*, *Ald*, *Idh*, *Mdh1*, *CG9467*, and *CG8460*. In mammalian β-cells, glucokinase and the glycolytic intermediates play important roles in glucose sensing (German 1993). Similarly, the enriched sugar metabolic enzymes in IPCs may participate in sugar sensing by IPCs.

Unexpectedly, the third cluster of enriched biological function relates to "skeletal muscle organ development" (Table 1). *Mef2* (**M**yocyte **e**nhancer **f**actor **2**) is the only gene that is annotated as muscle-specific, while most other genes have annotated neuronal and muscular roles, among them neuromuscular junction development. Mef2 is a transcription factor that functions in both neuron and muscle development in *Drosophila* and is required to control circadian remodeling of clock neurons (Lilly *et al.* 1995; Sivachenko *et al.* 2013). The majority of the genes (*unc-104*, *Frq1*, *Gs2*, *drl*, *Vap-33-1*) in this cluster are involved in synapse assembly and/or synaptic transmission, but have a relatively lower enrichment score due to the presence of *Mef2* in the list. IPCs are neurons, so we believed that "synapse organization" is a more proper representation of genes in cluster 3. IPCs presumably required such components for organizing IPC axonal terminals and for axonal transport needed for ILP release from these neurons.

Using HomoloGene from NCBI, we searched for mammalian homologs of fly IPC-enriched genes. Of the 193 IPC-enriched genes, 109 have clear mouse homologs (Table S5). Transcripts encoding *Drosophila* insulin-like peptides (*Ilp2*, *-3*, and *-5*) are the most enriched mRNAs in IPCs (>4000-fold compared with control neural tissue). This confirms that IPCs were included, and enriched, among the captured cells. mRNAs from *amon* and *ia2*, which encode *Drosophila* homologs of mammalian insulin-processing enzymes (Siekhaus and Fuller 1999; Rayburn *et al.* 2009) and insulin-secreting DCV components (Harashima *et al.* 2005; Kim *et al.* 2008), were also enriched (8- and 11-fold) in IPCs.

Screening for conserved genes that function in fly IPCs

Using available *UAS-RNAi* lines, 50 of the 193 IPC-enriched genes were tested for their influence on growth. Transgenes that encode RNAi were engineered to be active specifically in IPCs (Figure S1A). RNAi lines for individual genes from either the Vienna Drosophila RNAi Center (VDRC) or Transgenic RNAi Project (TRiP) collections were crossed with *Ilp2-Gal4*, and the adult progeny were examined for their weight (Dietzl *et al.* 2007; Ni *et al.* 2008) (Figure S1A). The *Ilp2* promoter drives gene expression in IPCs starting during late embryogenesis and continuing into adulthood (Rulifson *et al.* 2002; Slaidina *et al.* 2009) (Figure 1). RNAi inhibition in IPCs of *amon*, *foxo*, *Rab26*, *unc-104*, *hth*, *ald*, *Pkc98E*, *Vap-33-1*, *Vha26*, and *CG13506* had strong effects on adult fly size (>10% reduction) while inhibition of other genes had little or no effect (Figure S1A).

A recently published mRNA-seq database for genes expressed in adult mouse β-cells was used for cross-species comparison (Ku *et al.* 2012) (Table S5). In this study, the mouse homologs of *amon*, *foxo*, *Pkc98E*, *Rab26*, *Vha26*, *unc-104*, and *Vap-33-1* had high expression levels in pancreatic β-cells compared with other cell types. Amon is the fly homolog of mammalian proprotein convertase subtilisin/kexin type 2 (PCSK2), a processing enzyme for prohormones and neuropeptide precursors. In β-cells, PCSK2 is involved in cleavage of proinsulin to insulin and C-peptide (Davidson *et al.* 1988). Foxo/Foxo1 has been implicated in β-cell proliferation in the mouse pancreas (Ai *et al.* 2010). In flies, Foxo functions with JNK to control Ilp transcription in response to oxidative stress (Hwangbo *et al.* 2004; Wang *et al.* 2005). PRKCE, the mouse homolog of fly Pkc98E, is associated with insulin granules for exocytosis upon inositol hexakisphosphate stimulation (Hoy *et al.* 2003; Mendez *et al.* 2003). Mouse Rab37, a homolog of fly Rab26, associates

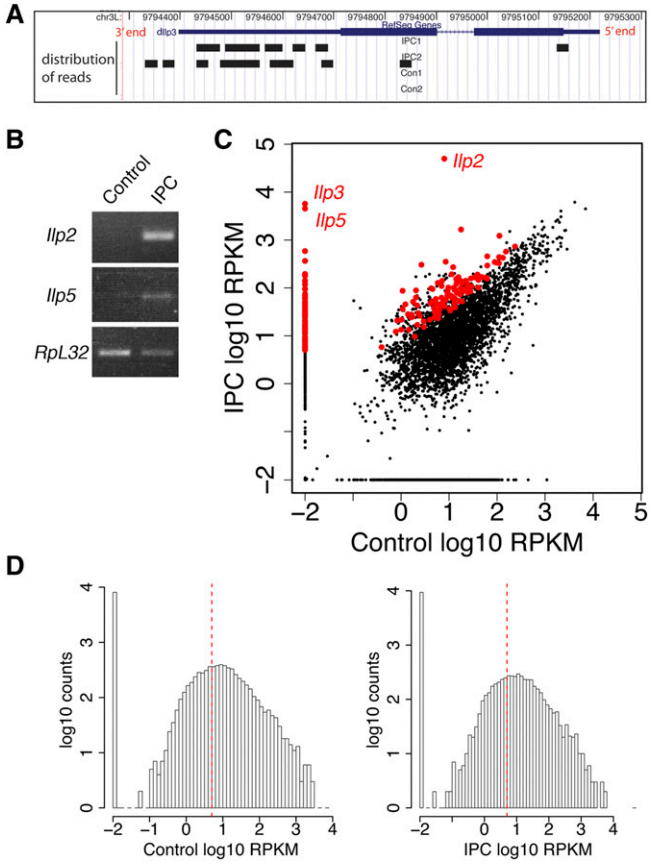

Figure 3 mRNA sequencing of IPCs and control neurons. (A) A 3′ bias of mRNA sequencing reads. Distribution of mRNA-seq reads along *Ilp3* mRNA as seen in the UCSC Genome Browser (Karolchik *et al.* 2003). RefSeq Gene track shows *Ilp3* mRNA structure. Wide blue bar: exons; narrow blue bar: 5′ and 3′ untranslated region; blue line: intron. Distribution of mRNA reads from IPC1, IPC2, control 1, and control 2 samples is shown as black bars in individual tracks. (B) RT-PCR validation of laser-captured IPCs. *Ilp2* and *Ilp5* mRNA levels were assayed in amplified mRNAs from captured IPCs and control neural tissues. The housekeeping gene *Ribosomal protein L32* (*RpL32*) was used as control. (C) Scatter plot of the mRNA-Seq expression data of IPCs and controls. Both the *x*- and the *y*-axis represent RPKM in $\log_{10}$ ratio. Red dots highlight IPC-enriched genes. A pseudo-count of 0.01 was added to RPKMs of all genes to avoid errors in log transformation of true. Thus, zero expression genes were represented as dots with expression of -2 in $\log_{10}$ on the plot. (D) Histograms of RPKM levels of genes expressed in controls and IPCs. The *x*-axis is $\log_{10}$ scale of gene expression measured in RPKM; the *y*-axis is gene counts in $\log_{10}$ scale. A pseudo-count of 0.01 was added to RPKMs of all genes to avoid errors in log transformation of true. The dashed red line represents RPKM = 5.

with insulin-secretory vesicles based on proteome analysis (Brunner *et al.* 2007), but its role in insulin secretion is unknown. Unc-104/Kif1a (a kinesin-3 microtubule motor), Vha26 (a proton transport ATPase), and Vap-33-1 (vesicle-associated membrane protein) have not been implicated in insulin secretion or β-cell proliferation. We chose Unc-104, a kinesin-3 microtubule motor, for further functional analysis, based upon the strong reduction in growth when it is inhibited in IPCs (Figure S1A).

Unc-104, a kinesin-3 family member, is required for neurite development and transporting ILP along the axons of IPCs

Depletion of *unc-104* mRNA from IPCs during development dramatically reduced adult size (by 27% using a VDRC line and 12% using a TRiP line) (Figure S1A). Unc-104 was previously characterized as an anterograde motor that transports cargos, including neuropeptide-filled and synaptotagamin-bearing vesicles, in the fly nervous system (Pack-Chung *et al.* 2007; Barkus *et al.* 2008). Insulin is packed in DCVs before release (Dean 1973; Takahashi *et al.* 2004), so in IPCs the ILPs could be transported by Unc-104. To test this possibility, we first determined how ILPs are transported in normal IPCs.

Immunofluorescence labeling of ILP2, one of the major ILPs, together with mCD8-labeled IPC neuronal processes showed that ILP2 is localized mainly in 14 cell bodies and some of their neurites (Figure 4A). To determine whether these ILP2-positive neurites have axon and/or dendrite features, we expressed axonal (Tau) and dendritic (Khc::nod) markers (Figure 4, B–D) (Rolls 2011). Tau-labeled IPC axonal bundles project contralaterally and posteriorly (Figure 4B, arrowhead), make a U-turn, and extend anteriorly (arrow) to terminals outside the brain. ILP2 resides mainly in these axonal projections (Figure 4A, white arrows; Figure 4B). The two main populations of Khc::nod-labeled dendritic arborizations extend laterally and posteriorly from the cell bodies (Figure 4C, yellow arrows). ILP2 was invisible, or at very low levels, in these neurite structures (Figure 4A, yellow arrows). The pattern of GFP-tagged DCV marker atrial natriuretic factor (ANF) in IPCs showed that DCV-carried neuropeptides are tightly associated with ILP2 granules in IPC cell bodies. This suggests that ILP2, like mammalian insulin, is packaged in DCVs for transport (Figure 4E) (Dean 1973; Rao *et al.* 2001; Takahashi *et al.* 2004). Since *Ilp2* mRNA is made in the cell bodies (Brogiolo *et al.* 2001; Rulifson *et al.* 2002), ILP2 protein carried in DCVs is transported out of the cell bodies and along the axonal projections of IPCs.

Depletion of Unc-104 from IPCs during early larval developmental stages reduced the number of IPCs, disrupted IPC morphology, and imposed ~1 day of developmental delay in adult eclosion (Figure 5A), indicating that *unc-104* is required during IPC development. Unc-104 is required for fly embryonic motor neuron synapse formation, larval synaptic terminal outgrowth, and dendrite morphogenesis of larval multidendritic neurons (Pack-Chung *et al.* 2007; Kern *et al.* 2013). In these past studies, a possible role of Unc-104 in insulin production would have been obscured by early developmental defects. To look specifically at Unc-104 function in ILP production, we employed *tub-Gal80^{ts}* as a temporal Gal4 switch. Gal80^{ts} inhibits Gal4 until increased temperature inactivates Gal80 and allows Gal4 to trigger gene transcription, in this case transcription of a gene encoding interfering *unc-104* mRNA. We allowed Unc-104 to

Table 1 Top-ranked biological processes represented by IPC-enriched transcripts

	FlyBase symbol	Gene name
	Enrichment score: 2.04	
Annotation cluster 1		
GO#0032868: response to insulin stimulus	*Ilp2*	Insulin-like peptide 2
GO#0032869: cellular response to insulin stimulus	*Ilp3*	Insulin-like peptide 3
GO#0043434: response to peptide hormone stimulus	*Ilp5*	Insulin-like peptide 5
GO#0008286: insulin-receptor-signaling pathway	*chico*	Insulin receptor substrate 1
GO#0032870: cellular response to hormone stimulus	*Ggamma30A*	G-protein gamma 30A
GO#0007169: transmembrane receptor protein tyrosine-kinase-signaling pathway	*SIFa*	IFamide
	Dh31	Diuretic hormone 31
	NPF	Neuropeptide F
	CCHa2-R	CCHamide-2 receptor
	Dh31-R	Diuretic hormone 31 receptor
	foxo	Forkhead box, subgroup O
	mAChR	Muscarinic acetylcholine receptor 60C
	Ms	Dromyosuppressin
	Hrs	Hepatocyte growth-factor-regulated tyrosine kinase substrate
	Mip	Myoinhibiting peptide precursor
	Ras85D	Ras oncogene at 85D
	drl	Derailed
	fog	Folded gastrulation
	Adar	Adenosine deaminase acting on RNA
	pix	Pixie
	Enrichment score: 1.67	
Annotation cluster 2		
GO#0006006: glucose metabolic process	*Pfk*	Phosphofructokinase
GO#0019318: hexose metabolic process	*Mdh2*	Malate dehydrogenase 2
GO#0005996: monosaccharide metabolic process	*Ald*	Aldolase
GO#0006096: glycolysis	*Idh*	Isocitrate dehydrogenase
GO#0006007: glucose catabolic process	*Mdh1*	Malate dehydrogenase
GO#0019320: hexose catabolic process	*CG9467*	Dmel_CG9467
	CG8460	Dmel_CG8460
	Vha26	Vacuolar H[+]-ATPase 26kD E subunit
	Vha55	Vacuolar H[+]-ATPase 55kD B subunit
	foxo	Forkhead box, subgroup O
	Enrichment score: 1.54	
Annotation cluster 3		
GO#0060538: skeletal muscle organ development	*unc-104*	Kinesin-like protein unc-104
GO#0048747: muscle fiber development	*Frq1*	Frequenin 1
GO#0007519: skeletal muscle tissue development	*Gs2*	Glutamine synthetase 2
GO#0014706: striated muscle tissue development	*Vap-33-1*	Dmel_CG5014
GO#0060537: muscle tissue development	*drl*	Derailed
GO#0050808: synapse organization	*foxo*	Forkhead box, subgroup O
	Mef2	Myocyte-enhancing factor 2

Each annotation cluster represents GO terms with similar biological functions determined by DAVID. Biological functional clusters were ranked based on the enrichment score. The top six GO terms that have the lowest *P*-values (most enriched) within each cluster are shown. All genes involved in each cluster are shown. Full list of the GO terms of each cluster is in Table S5.

function through late larval development at 18°, by which time IPC neurite structure has fully developed (Figure 1), and then changed the temperature to 29° for 24 hr to induce production of *unc-104* RNAi. This strategy successfully prevented occurrence of any visible defects in IPC development (Figure 5B). In control IPCs with functional Unc-104, low-level ILP2 was detected in the cell bodies. In contrast, 24-hr depletion of *unc-104* mRNA during the second–third larval instar transition caused striking accumulation of ILP2 in IPC cell bodies, as well as enrichment of ILP2 in neurites extending from the IPC cell bodies (Figure 5B). Quantitation showed that reducing *unc-104* function in IPCs caused

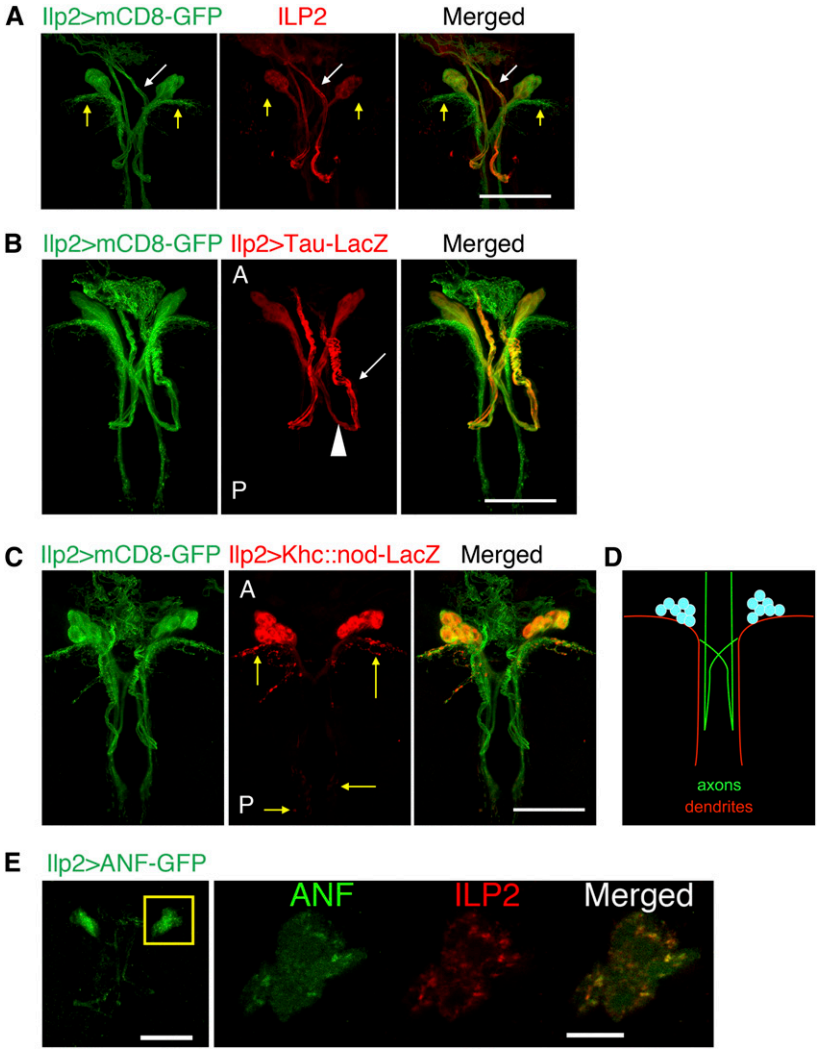

Figure 4 ILP2 is transported in DCVs along the axonal bundles in IPCs. (A) IPC neuronal structure from a third instar larval brain was labeled with *Ilp2->mCD8-GFP*. ILP2 localizes to some IPC neuronal projections (white arrow) but not to others (yellow arrows). (B–D) Localization of axonal (Tau) and dendritic (Khc::nod) markers in IPCs. In both figures, anterior (labeled with "A") is toward the top and posterior ("P") is toward the bottom. Arrowhead in B labels the portion of IPC axon bundles extending posteriorly from the cell bodies, and white arrow indicates, after the turn, IPC axons projecting anteriorly. Yellow arrows in C indicate the dendritic branches of IPCs. (D) Schematic of IPC polarity. (E) Localization of DCV in IPCs was examined by expressing exogenous ANF-GFP. Higher magnification of boxed region is shown for both ANF-GFP and ILP2 (single z optical section). Bars: 50 μm except in the zoomed-in image in E, where the bar represents 10 μm.

a twofold increase in ILP2 in the cell bodies of IPCs (Figure 5C). qPCR analysis indicated no obvious increase in brain *Ilp2* mRNA level after knockdown of *unc-104* for 24 hr (Figure S2). Thus insulin secretion was likely inhibited after depletion of *unc-104* mRNA.

Unc-104 is predominantly expressed in the nervous system in larval and adult flies (Chintapalli *et al.* 2007; Pack-Chung *et al.* 2007). To study the role of Unc-104 in IPCs, we examined the localization of Unc-104 protein in IPCs using tagged Unc-104 produced in IPCs (*Ilp2 > Unc-104-mCherry*, Figure 5D). Expression of this tagged Unc-104 in the nervous system is sufficient to rescue *unc-104* mutant phenotypes (Pack-Chung *et al.* 2007; Kern *et al.* 2013). In IPCs, Unc-104-mCherry strongly colocalized with axons (Figure 5D). Unc-104-mCherry was also in IPC dendrites, but at a much lower level compared to axons. A similar pattern of Unc-104 localization was observed when GFP-tagged Unc-104 was expressed in IPCs (Figure 5E) (Barkus *et al.* 2008).

When *unc-104* was depleted, ILP2 accumulated in IPC axons. The accumulation was limited to regions proximal to the cell bodies (Figure 5B, bottom). In view of the known role of Unc-104 in transporting DCVs in other neurons (Pack-Chung *et al.* 2007; Barkus *et al.* 2008), the localization of Unc-104 in IPCs and their axonal processes is consistent with a role for the motor protein in transporting ILP2 in DCVs along axons, especially in regions proximal to the cell bodies.

IPC-specific production of Rab DN proteins identifies Rab1 as a potent growth factor and hemolymph sugar modulator

To identify additional proteins involved in fly ILP production, 29 dominant-negative fly Rab constructs (*UAS-Rab DN*) were screened by crossing at least one line for each *Rab* gene to the *Ilp2-Gal4* driver (Rulifson *et al.* 2002; Zhang *et al.* 2007). Among 43 lines tested, only IPC-specific expression of *Rab1-DN* resulted in a dramatic (>40%) reduction in adult fly weight (Figure 6A and Figure S1B). The other *Rab-DN* lines, including *Rab27-DN*, had little effect on fly weights when expressed in IPCs (Figure S1B). *Rab27* is the fly ortholog of mammalian *Rab27a*, which is involved in insulin

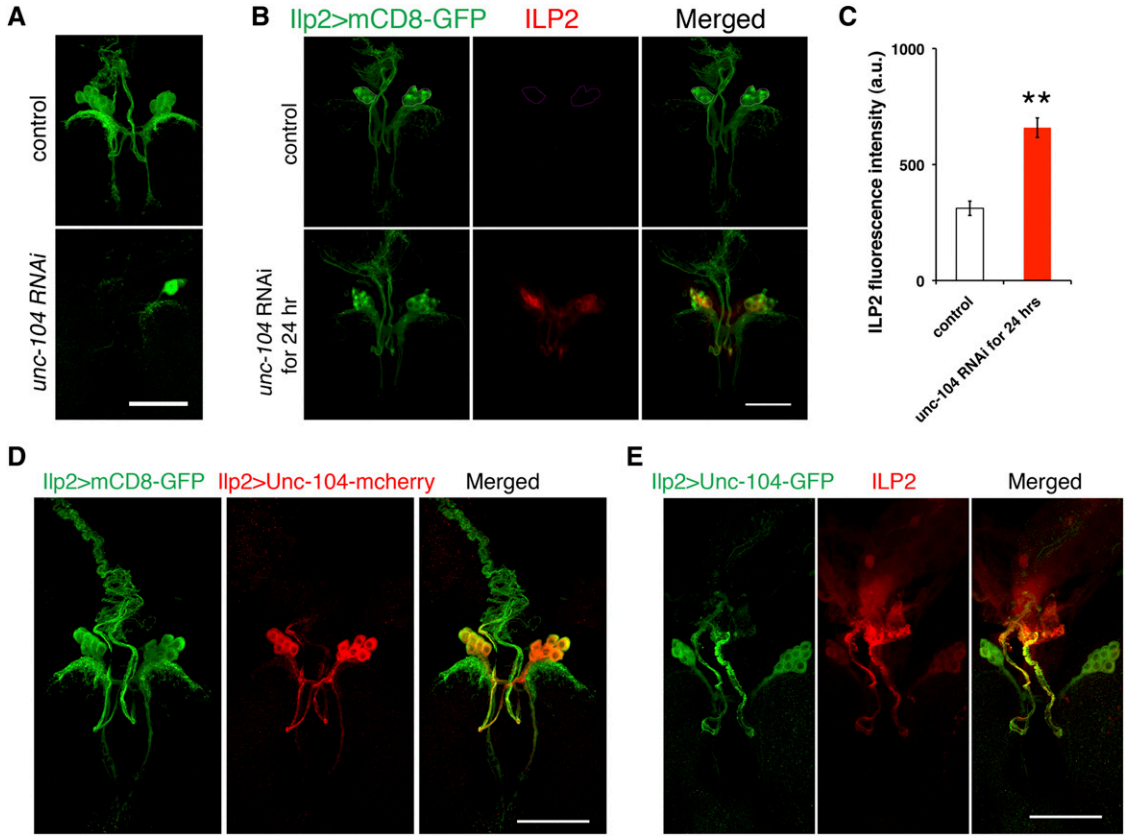

Figure 5 Unc-104 is localized to axons of IPCs and is required for IPC development and ILP2 secretion. (A) Control (*Ilp2* > w^{1118}, VDRC GD line control, #60000) and *Ilp2* > *unc-104 RNAi* (VDRC line #23465) third instar brains were dissected. *Ilp2* > *mCD8-GFP* (green) indicates the whole IPC neural structure. (B and C) ILP2 fluorescence intensities in the brain IPC cell bodies were compared between control (*tubGal80*^{ts}, *Ilp2* > w^{1118}, VDRC GD line control, #60000, n = 9 brains) and *unc-104* knockdown (n = 9 brains) in IPCs for 24 hr (*tubGal80*^{ts}, *Ilp2* > *unc-104 RNAi*). The images were taken with the same laser settings and manipulated in the same way. IPC cell bodies are outlined in the circle in control. (D and E) Localization of Unc-104 in IPCs was examined by expressing exogenous *Unc-104-mCherry* or *Unc-104-GFP*. *Ilp2* > *mCD8-GFP* (green) indicates the whole IPC neural structure. Bars, 50 μm. Error bars: SEM, $^{**}P < 0.01$.

granule exocytosis (Yi *et al.* 2002). In the larval brain lobes, *Rab27* is expressed in the mushroom bodies and developing antennal lobes, but not in IPCs (Chan *et al.* 2011), which explains why expression of *Rab27-DN* in IPCs did not cause a growth phenotype. Expressing *Rab26-DN* in IPCs had a weaker effect on growth inhibition (7% reduction in size), compared with a 20% reduction in size achieved with *Rab26 RNAi*, suggesting that the DN construct is less effective than the RNAi construct (Figure S1). Rab1 is expressed ubiquitously in the brain including in all 14 IPCs (Figure 6C) (Chan *et al.* 2011). Producing Rab1-DN in IPCs dramatically reduced pupal size to only 61% of the controls, in keeping with the RNAi data (Figure 6B and Figure S3A).

Reducing ILP production or secretion inhibits fly growth and developmental progression (Geminard *et al.* 2009; Zhang *et al.* 2009; Gronke *et al.* 2010). We tested whether inhibiting Rab1 in IPCs affects developmental timing. Flies producing Rab1-DN in IPCs eclosed and pupated, on average, ~2 days later than control flies (Figure 6, D and E). One direct consequence of reduced ILP production or secretion is elevated levels of circulating sugars in hemolymph (Rulifson *et al.* 2002). With larvae producing Rab1-DN in IPCs, hemolymph levels of trehalose and glucose were elevated compared to control larvae (Figure 6F). The average combined trehalose and glucose levels for control larvae and *Ilp2* > *Rab1-DN* larvae were 2372 and 2904 mg/dl, respectively. The values of carbohydrate concentration for the *Rab1-DN* larvae resembled the levels of IPC-ablated larvae (Rulifson *et al.* 2002). This elevated sugar level, together with developmental delay and growth inhibition caused by Rab1-DN produced in IPCs, suggests that Rab1 promotes ILP production by IPCs.

Rab1 is required for IPC dendrite morphogenesis and ILP transport out of the IPC cell bodies

To explore the mechanism by which Rab1-DN inhibits ILP production, we first looked for any IPC developmental defects caused by constitutive inhibition of Rab1 in IPCs. IPC morphology and cell number were examined using mCD8-GFP and a RFP-conjugated nuclear marker, combined with Rab1-DN produced in the IPCs. Under these conditions, there were fewer IPCs in these larvae (Figure 7, A and B). The average IPC count was reduced from 14 ± 0.0 in wild-type larvae to 8.7 ± 0.4 in *Ilp2* > *Rab1-DN* larvae.

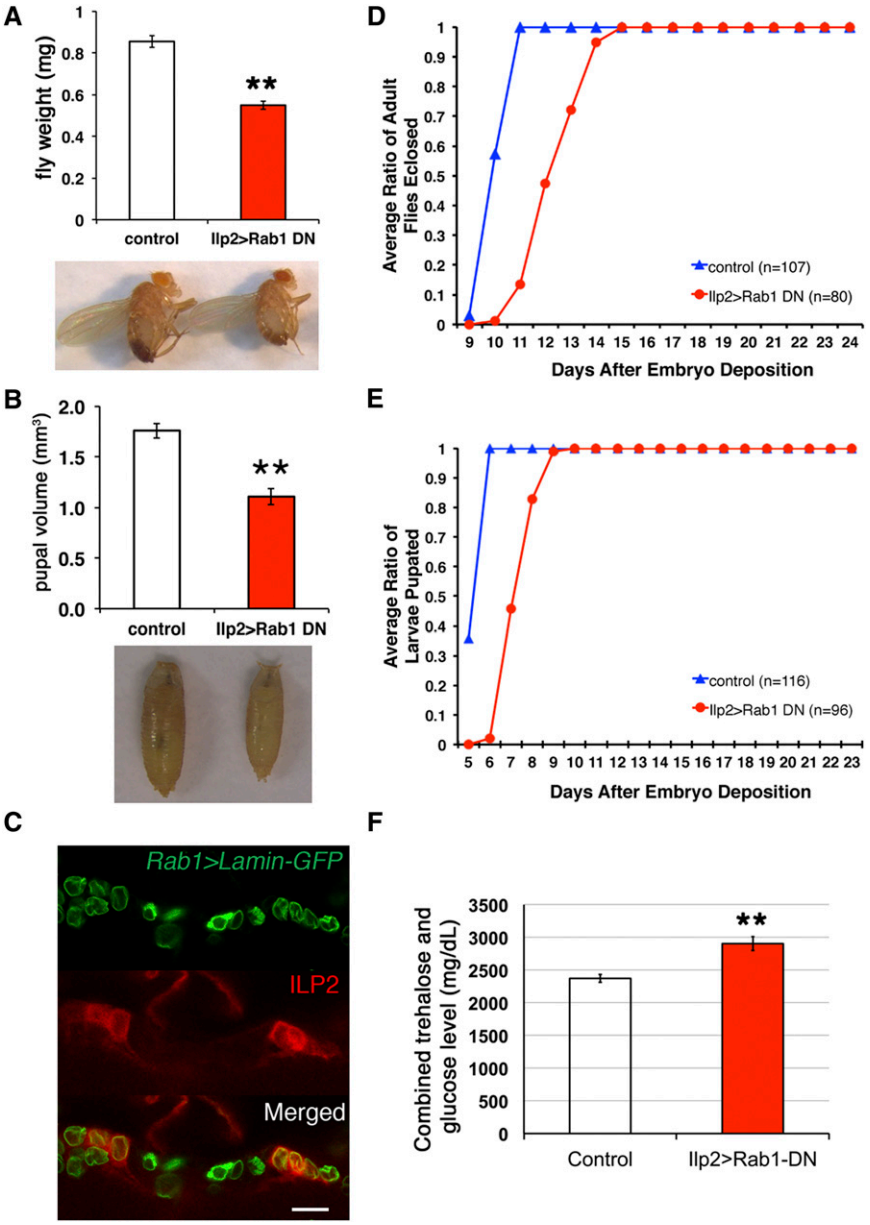

Figure 6 Rab1 is required in IPCs for normal animal growth and development. (A and B) Adult weights and pupal volume were compared between control flies (*Ilp2-Gal4* > *yw*, *n* = 153 flies, *n* = 5 pupae) and flies expressing *Rab1-DN* in IPCs (*Ilp2* > *Rab1-DN*, *n* = 138 flies, *n* = 6 pupae). (C) In a single confocal optical section, IPCs were labeled with anti-ILP2 antibody, and *Rab1*-expressed cells were labeled with *Rab1* > *Lamin-GFP*. The other IPCs that were not displayed in this optical section also expressed *Rab1*. Bar, 20 μm. (D and E) Developmental time points of the onset of metamorphosis and adult eclosion were compared between control flies and flies expressing *Rab1-DN* in IPCs. (F) Combined trehalose and glucose level in the third instar larval hemolymph was compared between control (*n* = 12 pooled hemolymph samples) and *Ilp2-Gal4* > *Rab1-DN* flies (*n* = 10 pooled hemolymph samples). Data were represented as mean ± SEM, $^{**}P < 0.01$.

IPC neuronal morphology was dramatically disrupted. In *Ilp2* > *Rab1-DN* larvae, dendritic arborizations were missing (Figure 7A, white arrows), while the axonal bundles were mostly intact. To specifically examine whether Rab1 controls ILP production, we employed the Gal80^{ts} stretegy described earlier to inhibit Rab1 after IPC neurite structures had fully developed. As with *unc-104* inhibition, late inhibition of Rab1 for 24 hr with the tub-Gal80^{ts} system avoided IPC developmental defects but caused a 1.6-fold increase in ILP2 level in IPC cell bodies (Figure 7, C and D). The level of ILP2 was reduced in the axonal projections that connect the IPC cell bodies, suggesting that ILP2 was trapped in cell bodies rather than transported along axons. qPCR assays indicated no obvious changes in brain *Ilp2* mRNA level after expression of *Rab1-DN* for 24 hr (Figure S2). As an alternative approach to inhibit Rab1 function, we expressed *Rab1 RNAi* using the *Ilp2-Gal4* driver. At 29°, the RNAi caused strong accumulation of ILP2 in IPC cell bodies but left IPC morphology intact (Figure S3, B–D). Brains expressing *Rab1 RNAi* had the normal 14 IPCs, yet the RNAi reduced fly weight by 20%. The RNAi effect was milder than the effect of *Rab1-DN* (Figure S3A and Figure 6A). *Rab1 RNAi* in IPCs caused only a slight developmental delay (about one-half day delayed for pupation and adult eclosion) and allowed axons and dendrites of IPCs to be formed and maintained properly. There was some loss of left–right symmetry (Figure S3B), perhaps as a consequence of perturbing global growth. Despite the mild effects on development and IPC morphology, *Rab1 RNAi* caused a doubling of ILP2 accumulation in IPC cell bodies (Figure S3, C and D). Both types of depletion of Rab1 function suggest a role for Rab1 in controlling intracellular trafficking of ILP2.

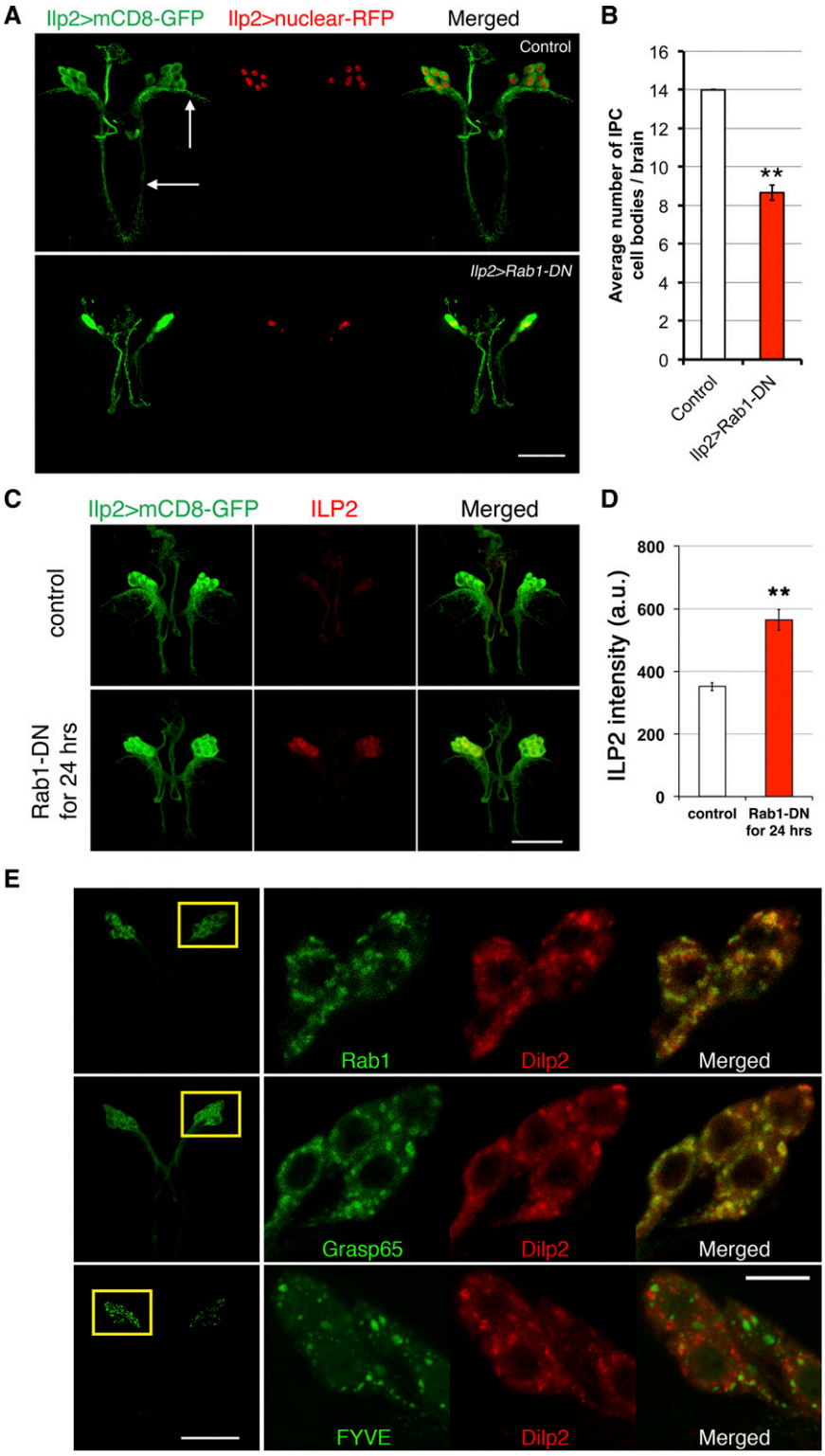

Figure 7 Rab1 colocalizes with ILP2 granules and is required for IPC development and ILP2 transport. (A) IPC neurite structure and nuclei were labeled with *Ilp2 > mCD8-GFP* and *Ilp2 > nls-RFP* in third instar larval brains. (Top) The white arrows indicate the dendrites of control IPCs (*Ilp2-Gal4 > yw*), which were missing in *Ilp2-Gal4 > Rab1-DN* brains. (B) Quantification of IPC cell numbers (based on *Ilp2 > nls-RFP*-labeled nuclei) indicated a reduction (five to six) in *Ilp2-Gal4 > Rab1-DN* brains ($n = 9$ brains; for controls, $n = 10$). (C and D) ILP2 fluorescence intensities in the brain IPC cell bodies were compared between control (*tubGal80^{ts}*, *Ilp2 > yw*, $n = 10$ brains) and Rab1 inhibition ($n = 14$ brains) in IPCs for 24 hr (*tubGal80^{ts}*, *Ilp2 > Rab1-DN*). The images were taken with the same laser settings and manipulated in the same way. (E) Labeling of Rab1 (*Ilp2 > Rab1-YFP*), a Golgi marker (*Ilp2 > Grasp65-GFP*), or an endosome marker (*Ilp2 > FYVE-GFP*) in combination with ILP2 staining. The left column (bottom magnification) shows the localization of GFP/YFP-tagged proteins as a projection of z-stacks. Rab1- and FYVE-labeled endosomes were localized almost exclusively in the cell bodies, while Grasp65-labeled *cis*-Golgi distributed in both the IPC cell bodies and the axons. Boxed regions are shown in higher magnification in the right columns. Rab1-YFP, Grasp-GFP, FYVE-GFP, and ILP2 all had punctate localization patterns in IPCs. For examination of colocalization between vesicles/granules, single z optical sections were shown. Bars, 50 μm except in the zoomed-in images in E, where the bar represents 10 μm. Error bars: SEM, $^{**}P < 0.01$.

When Rab1 is inhibited in IPCs, ILP secretion is inhibited during transit from cell bodies to the axonal tracts. To investigate whether Rab1 directly influences ILP transport in IPCs, ILP2 was labeled with antibodies in wild-type IPCs expressing Rab1-YFP. Rab1-YFP was localized within IPC cell bodies with very low fluorescence in IPC axons or dendrites (Figure 7E). Rab1-YFP and ILP2 immunofluorescent labeling displayed punctate patterns in IPC cell bodies. Strikingly, the majority of ILP2 punctae overlapped with Rab1 punctae, suggesting that Rab1-containing vesicles directly transport ILP granules along the route of ILP secretion.

Rab1 controls ER-to-Golgi transport (Stenmark 2009), so we investigated whether ILP2 granules reside in the Golgi. Producing the GFP-labeled Golgi marker Grasp65 in IPCs revealed punctate Golgi patterns that colocalized with ILP2 granules (Figure 7E). As a negative control, the endosome marker FYVE-GFP was produced in IPCs. The FYVE-labeled endosomes were in a punctate pattern, like Grasp65-GFP and Rab1-YFP, but had few overlaps with ILP2 granules. These data, together with the elevated ILP levels in IPCs after Rab1 inhibition, suggested that ILP is delivered by Rab1 to the Golgi in IPC cell bodies. The failed delivery of ILPs outside the cell bodies, due to Rab1 inhibition, results in failed secretion.

Discussion

Drosophila brain IPCs regulate development, growth, metabolism, stress resistance, life span, feeding, locomotor activity, olfactory sensitivity, sleep, and ethanol sensitivity in response to internal physiological and external nutritional signals (Nassel 2012). Until now, only a handful of genes were known to function in IPCs. By combining LCM, RNA-seq, two *UAS-RNAi* libraries, and our *UAS-Rab-DN* collection, we systematically screened for genes that are important for IPC function. Among genes that rendered IPC-specific phenotypes when inhibited in IPCs, we focused on *unc-104* and *Rab1* and investigated their roles in ILP secretion and IPC development.

Conservation between mammalian pancreatic β-cells and fly IPCs

Among the neurons, glial cells, intestinal muscle cells, adipocytes, and salivary gland cells that can produce ILPs in flies (Brogiolo *et al.* 2001; Ikeya *et al.* 2002; Miguel-Aliaga *et al.* 2008; Okamoto *et al.* 2009; Chell and Brand 2010; O'Brien *et al.* 2011; Sousa-Nunes *et al.* 2011), brain IPCs are the best-characterized. Several lines of evidence indicate that *Drosophila* brain IPCs and mammalian pancreatic β-cells share functional and physiological similarities: (1) Genetic ablation of fly IPCs or deletion of fly ILPs results in metabolic phenotypes similar to mammals with β-cell/insulin deficiency (Brogiolo *et al.* 2001; Ikeya *et al.* 2002; Rulifson *et al.* 2002; Zhang *et al.* 2009; Gronke *et al.* 2010). (2) Fly ILPs and mammalian insulin carry out their functions by activating a conserved signaling pathway in target tissues (Baker and Thummel 2007). (3) In *Drosophila*, brain IPCs and adipokinetic hormone-producing cells are physically connected through neuronal projections and in this sense at least are functionally analogous to pancreatic β- and α-cells (Kim and Rulifson 2004). (4) β-Cells and fly IPCs respond to Leptin/Leptin-like cytokine secreted from adipose tissue to regulate ILP release (Kieffer *et al.* 1997; Rajan and Perrimon 2012).

Phylogenetic analyses of insulin-producing cells suggest that mammalian β-cells and fly IPCs have common evolutionary origins or have different origins but have undergone convergent evolution (Arntfield and Van Der Kooy 2011). Mammalian β-cells arise from the endoderm (Jensen 2004), and fly IPCs are neurons arising from the ectoderm (Wang *et al.* 2007). Fly IPCs have long axons requiring extensive transport of vesicles, while β-cells have no axons. Yet phylogenic analyses of insulin-expressing cells indicate that neurons evolved to secrete insulin before there were β-cells, creating a puzzle about the evolutionary origin of β-cells (Arntfield and Van Der Kooy 2011). In jellyfish, insulin is produced only by neurons (Davidson *et al.* 1971). In *Caenorhabditis elegans* and in *Drosophila*, insulin is produced by neurons and by endoderm-derived cells (Brogiolo *et al.* 2001; Rulifson *et al.* 2002; Li *et al.* 2003). The insulin-producing cells in a worm's nervous system and intestine respond to food intake to control development, life span, and stress resistance (Li *et al.* 2003; Iser *et al.* 2007).

Pancreatic β-cells have some similarities to neurons. From the perspective of physiology, (1) β cells and neurons pack their signaling peptides into secretory granules and release them using action potentials (Rorsman and Renstrom 2003). (2) Hypothalamic neurons can sense blood glucose levels (Lam *et al.* 2005), as β-cells do. From the perspective of gene expression, (1) β-cells express certain "neural-specific" genes, which encode sodium channels, neurofilaments, neurotransmitters (such as GABA), and their receptors (Escurat *et al.* 1991; Philipson *et al.* 1993; Glassmeier *et al.* 1998; Adeghate and Ponery 2002; Xu *et al.* 2006). (2) Neurons and β-cells do not express the gene encoding the neuron-restrictive silencing factor/repressor silencing transcription factor, a negative regulator of neuron fate that is made only in non-neuronal cells (Atouf *et al.* 1997). For all these reasons, β-cells and insulin-expressing neurons may share properties and proteins useful for controlling insulin production and secretion.

By analyzing the IPC transcriptome using LCM and mRNA sequencing, we found a group of IPC-enriched mRNAs that are orthologs of mammalian genes active during insulin production and secretion. Larval-stage-specific *Ilp*s (*Ilp2*, *Ilp3*, and *Ilp5*) were found, as expected, and we detected enrichment of *amon*, *ia2*, and *Pkc98E* mRNAs, which encode *Drosophila* orthologs of key mammalian insulin-processing enzymes, DCV components, and signal transducers that control insulin secretion (Settle *et al.* 1995; Siekhaus and Fuller 1999; Hoy *et al.* 2003; Mendez *et al.* 2003; Dong *et al.* 2006; Rayburn *et al.* 2009). Many other IPC-enriched genes have mouse orthologs that are preferentially transcribed in pancreatic β-cells (Ku *et al.* 2012). This provided good evidence that our captured samples were highly enriched in IPCs and strengthened the evidence for conservation between fly IPCs and mammalian β-cells. Functional tests indicated that at least 20% (10 of 50) of the IPC-enriched genes that have mammalian orthologs are required in IPCs for proper *Drosophila* body size to be attained. RNAi with expression of any of these genes in IPCs strongly (>10%) reduced growth. Therefore, the combination of LCM and RNA-seq is a powerful and sensitive

method for characterizing the transcriptome of a specific cell type, such as IPCs, that is present in limited cell numbers in the brain.

In addition to ILPs, four neuropeptide genes were enriched in our IPC samples: *Myoinhibiting peptide precursor* (*Mip*), *Dromyosuppressin* (*Dms*), *neuropeptide F* (*npf*), and *IFamide* (*IFa*). These may be contaminants from adjacent cells (Park *et al.* 2008). Since our starting materials were only 23 captured cells for each IPC sample, if one of the neuropeptide mRNAs is at a higher level (*e.g.*, >100-fold) compared to average brain cells, it may have been purified along with IPC mRNAs. Since we used third instar larval IPCs for transcriptome analysis, mRNAs for G-protein-coupled receptors, membrane channels, and transporter proteins that are abundant in IPCs earlier in development may not be present among our enriched mRNAs. Larvae undergo developmental transitions in the third instar stage that require ecdysone and involve metabolic changes. By capturing gene expression during that time we sampled a larger range of cell properties and conditions than doing the same analysis of adult IPCs.

IPC neuronal polarity and neurite development

Our studies and prior work suggest that ILP2 is synthesized in IPC cell bodies and transported out of the cell bodies mainly along Tau-labeled axonal projections to IPC axonal terminals, where ILP2 is released (Brogiolo *et al.* 2001; Ikeya *et al.* 2002; Rulifson *et al.* 2002; De Velasco *et al.* 2007; Geminard *et al.* 2009). ILP2 is also released within the brain (Bader *et al.* 2013). By following IPCs during larval development, we observed that IPC axons and dendrites extend over greater distances until the early third instar larval stage. The neurite extension of IPCs is required to compensate for the size increase of brain lobes, so that connections between IPCs and other brain regions such as subesophageal ganglion are maintained (Rulifson *et al.* 2002; De Velasco *et al.* 2007). IPC dendrite extension and more extensive dendritic arborization might also be required to form new neuronal connections with other neurons, thus adjusting to new developmental and physiological needs.

Unc-104 in ILP transport in IPCs

Two regulators of ILP production, Unc-104 and Rab1, emerged as the strongest regulators from our screens. Strict regulation of ILP secretion is required to adjust downstream insulin signaling to food availability and metabolic status. Precise control is achieved through regulatory steps in IPCs: sensing of neuronal or hormonal signals, control of ILP secretion machinery by the signals, directed transport of ILPs to the IPC axonal terminal, and final release of ILP out of IPCs. Based upon our experiments, both Unc-104 and Rab1 are involved in directed transport of ILPs.

Unc-104 in worms and flies, and its mammalian homolog Kif1a, are anterograde motor proteins that transport DCVs along axons (Okada *et al.* 1995; Zahn *et al.* 2004; Pack-Chung *et al.* 2007; Barkus *et al.* 2008; Lo *et al.* 2011). DCVs exist in different cell types. In neurons, DCVs are responsible for transporting, processing, and secreting neuropeptide cargos. In pancreatic β-cells, insulin is packed into DCVs. The movement and secretion of insulin-containing DCVs to β-cell surfaces is a Ca^{2+}-dependent process that requires kinesin heavy chain movement along microtubules (Meng *et al.* 1997; Donelan *et al.* 2002; Cui *et al.* 2011). It is currently unknown whether other kinesin family proteins contribute to insulin-containing DCV movement and secretion. Our study shows that a kinesin 3 family protein, Unc-104, transports insulin granules along the axons of IPCs. ILP2 colocalizes with DCVs in IPC cell bodies. We observed Unc-104 and ILP2 distributed along IPC axons. Reducing *unc-104* function using two different small interfering RNAs (siRNAs) caused accumulation of ILP2 in cell bodies and in their proximal axonal projections. Consistent with a role for fly Unc-104 in transporting insulin-like peptides, *C. elegans* Unc-104 transports fluorescently tagged insulin-like protein 22 and IA-2 in motor neurons (Goodwin *et al.* 2012). Mammalian *Kif1a*'s role in insulin transport and secretion has not been reported. *Kif1a* mutant mice die soon after they are born due to severe motor and sensory defects (Yonekawa *et al.* 1998). They exhibit defects in the localization of synaptic vesicle precursors. Whether newborn *Kif1a* mutant mice have diabetic symptoms has not been reported.

Rab1 in ILP transport in IPCs

The small GTPase Rab1 regulates membrane trafficking within early Golgi compartments and in the ER–Golgi transition. In *Drosophila*, Rab1 was first described as a contributor in the maintenance of photoreceptor cell structure by mediating vesicle transport between the rough ER and Golgi body (Satoh *et al.* 1997). Our study shows that Rab1 is expressed ubiqutously in the fly brain, including IPCs. The specific effect with only *Rab1-DN* but not other *Rab-DN*s when expressed in IPCs shows that Rab1-DN interferes specifically with endogenous Rab1 function. It also rules out an alternative interpretation that Rab1-DN titrates some endogenous protein such as a GEF that works on multiple Rabs, one of which is the real regulator, in addition to Rab1. Inhibiting Rab1 function through dominant-negative or siRNA constructs caused accumulation of ILP2 in cell bodies and substantially reduced ILP2 in IPC axons. YFP-tagged Rab1 is localized predominantly in the cell bodies and exhibits a tight association with ILP2 granules cytologically. A recent study of the silkworm *Bombyx mori* showed that Rab1 is restricted to a small number of neurons in the brain, where it colocalizes with Bombyxin, an insulin family peptide, in the pars intercerebralis area (Uno *et al.* 2013). Proteomic analysis showed that Rab1 is enriched in immunopurified β-cell insulin granules (Hickey *et al.* 2009). Rab1 may be conserved as a critical molecule needed for insulin production.

Unc-104 and Rab1 in IPC development

In addition to their roles in ILP production, Unc-104 and Rab1 are required for IPC development. Constitutive depletion of

unc-104 mRNA from IPCs using *Ilp2-Gal4* resulted in severe disruption of IPC axons and dendrites and dramatically reduced IPC cell numbers as detected by *Ilp2 > mCD8-GFP*. Since IPCs are post-mitotic neurosecretory cells and *Ilp2* mRNA is produced only after IPC differentiation (Wang *et al.* 2007; Hwang and Rulifson 2011), *Ilp2-Gal4*-driven *unc-104 RNAi* does not interfere with the initial formation and specification of IPCs during late embryogenesis. Therefore, the observed reduction in IPC cell numbers at late larval stages comes from cell death during larval development. This phenotype is consistent with the observation that *Kif1a* mutant mice, and cultures of *Kif1a* mutant neurons, exhibit marked neuronal degeneration and death, which could be caused by insufficient neural stimulation due to disrupted neural connections (Yonekawa *et al.* 1998). Given the roles that Unc-104 plays in fly motor neuron and multidendritic neuron development (Pack-Chung *et al.* 2007; Kern *et al.* 2013), the axonal and dendritic morphology disruption seen in IPCs could be an initial neurite outgrowth defect, a later maintenance defect, or a combination of both.

We have found that constitutive inhibition of *Rab1* in IPCs, using a dominant-negative protein, resulted in disruption of IPC dendrites to a lesser extent than *unc-104 RNAi*. Rab1 functions in ER-to-Golgi transport, so this preferential disruption of IPC dendrites over IPC axons could be explained if IPC dendrites, like those of fly "da" neurons and rodent hippocampal neurons, are more sensitive to the reduction of ER-to-Golgi transport than IPC axons (Ye *et al.* 2007). *Rab1-DN* induced cell death during IPC development, although less severely than *unc104 RNAi*. The milder phenotypes with respect to neuron viability and neurite morphology in IPCs producing *Rab1-DN* compared to IPCs expressing *unc-104 RNAi* are consistent; a milder defect in neurite morphology may underlie a milder defect in neuron viability. Alternatively, Rab1-DN might cause accumulation of cytotoxic components such as misfolded α-synucleins in IPCs, which could underlie the loss of IPCs (Cooper *et al.* 2006).

Proteins like Rab1 and Unc-104 have multiple functions in a variety of cell types. Using cell-type-specific interference, we have explored their roles in production and transport of insulin-like peptides and determined the cellular and whole-organism phenotypes associated with their damaged functions. These proteins join an important list of critical factors needed for the controlled production and release of insulin-family proteins.

Acknowledgments

We thank the Transgenic RNAi Project at Harvard Medical School (National Institutes of Health/National Institute of General Medical Sciences R01-GM084947), the Vienna Drosophila Research Center, and the Bloomington Stock Center for providing transgenic RNAi and other fly stocks used in this study. We appreciate the generous help from Pierre Leopold, Eric Rulifson, Ping Shen, Tom Schwarz, Bill Saxton, Robin Hiesinger, and Liqun Luo, who provided flies and antibodies; Liqun Luo for supporting M.L.S. and Ziming Weng, Phil Lacrout, and Arend Sidow in flow-cell preparation, sequencing, and data processing; Sam Gu for help and suggestions on preparing mRNA-seq libraries for sequencing; Kaye Suyama, Weiwei Chen, and Dan Gui for helping with fly stock maintenance; and Virginia Walbot for sharing with us the cryostat and LCM in her lab. We also thank Liqun Luo, Tom Hartl, Ljiljana Milenkovic, and Alex Brown for critical comments on the manuscript. Research in the Kim lab was supported by the Howard Hughes Medical Institute (HHMI). J.C. was supported by Stanford University's Bio-X Interdisciplinary Initiatives Seed Grant. J.N. is a postdoctoral fellow, and S.K.K. and M.P.S. are Investigators of the HHMI.

Literature Cited

Adams, M. D., S. E. Celniker, R. A. Holt, C. A. Evans, J. D. Gocayne *et al.*, 2000 The genome sequence of Drosophila melanogaster. Science 287: 2185–2195.

Adeghate, E., and A. S. Ponery, 2002 GABA in the endocrine pancreas: cellular localization and function in normal and diabetic rats. Tissue Cell 34: 1–6.

Ai, J., J. Duan, X. Lv, M. Chen, Q. Yang *et al.*, 2010 Overexpression of FoxO1 causes proliferation of cultured pancreatic beta cells exposed to low nutrition. Biochemistry 49: 218–225.

Arntfield, M. E., and D. van der Kooy, 2011 β-Cell evolution: how the pancreas borrowed from the brain: the shared toolbox of genes expressed by neural and pancreatic endocrine cells may reflect their evolutionary relationship. Bioessays 33: 582–587.

Atouf, F., P. Czernichow, and R. Scharfmann, 1997 Expression of neuronal traits in pancreatic beta cells. Implication of neuron-restrictive silencing factor/repressor element silencing transcription factor, a neuron-restrictive silencer. J. Biol. Chem. 272: 1929–1934.

Bader, R., L. Sarraf-Zadeh, M. Peters, N. Moderau, H. Stocker *et al.*, 2013 The IGFBP7 homolog Imp-L2 promotes insulin signaling in distinct neurons of the Drosophila brain. J. Cell Sci. 126: 2571–2576.

Bai, H., P. Kang, and M. Tatar, 2012 Drosophila insulin-like peptide-6 (dilp6) expression from fat body extends lifespan and represses secretion of Drosophila insulin-like peptide-2 from the brain. Aging Cell 11: 978–985.

Baker, K. D., and C. S. Thummel, 2007 Diabetic larvae and obese flies-emerging studies of metabolism in Drosophila. Cell Metab. 6: 257–266.

Barkus, R. V., O. Klyachko, D. Horiuchi, B. J. Dickson, and W. M. Saxton, 2008 Identification of an axonal kinesin-3 motor for fast anterograde vesicle transport that facilitates retrograde transport of neuropeptides. Mol. Biol. Cell 19: 274–283.

Baugh, L. R., A. A. Hill, E. L. Brown, and C. P. Hunter, 2001 Quantitative analysis of mRNA amplification by in vitro transcription. Nucleic Acids Res. 29: E29.

Bohni, R., J. Riesgo-Escovar, S. Oldham, W. Brogiolo, H. Stocker *et al.*, 1999 Autonomous control of cell and organ size by CHICO, a Drosophila homolog of vertebrate IRS1–4. Cell 97: 865–875.

Brogiolo, W., H. Stocker, T. Ikeya, F. Rintelen, R. Fernandez *et al.*, 2001 An evolutionarily conserved function of the Drosophila

insulin receptor and insulin-like peptides in growth control. Curr. Biol. 11: 213–221.
Brunner, Y., Y. Coute, M. Iezzi, M. Foti, M. Fukuda *et al.*, 2007 Proteomics analysis of insulin secretory granules. Mol. Cell. Proteomics 6: 1007–1017.
Chan, C. C., S. Scoggin, D. Wang, S. Cherry, T. Dembo *et al.*, 2011 Systematic discovery of Rab GTPases with synaptic functions in Drosophila. Curr. Biol. 21: 1704–1715.
Chell, J. M., and A. H. Brand, 2010 Nutrition-responsive glia control exit of neural stem cells from quiescence. Cell 143: 1161–1173.
Chintapalli, V. R., J. Wang, and J. A. Dow, 2007 Using FlyAtlas to identify better Drosophila melanogaster models of human disease. Nat. Genet. 39: 715–720.
Colombani, J., S. Raisin, S. Pantalacci, T. Radimerski, J. Montagne *et al.*, 2003 A nutrient sensor mechanism controls Drosophila growth. Cell 114: 739–749.
Cooper, A. A., A. D. Gitler, A. Cashikar, C. M. Haynes, K. J. Hill *et al.*, 2006 Alpha-synuclein blocks ER-Golgi traffic and Rab1 rescues neuron loss in Parkinson's models. Science 313: 324–328.
Cui, J., Z. Wang, Q. Cheng, R. Lin, X. M. Zhang *et al.*, 2011 Targeted inactivation of kinesin-1 in pancreatic beta-cells in vivo leads to insulin secretory deficiency. Diabetes 60: 320–330.
Davidson, H. W., C. J. Rhodes, and J. C. Hutton, 1988 Intraorganellar calcium and pH control proinsulin cleavage in the pancreatic beta cell via two distinct site-specific endopeptidases. Nature 333: 93–96.
Davidson, J. K., S. Falkmer, B. K. Mehrotra, and S. Wilson, 1971 Insulin assays and light microscopical studies of digestive organs in protostomian and deuterostomian species and in coelenterates. Gen. Comp. Endocrinol. 17: 388–401.
Dean, P. M., 1973 Ultrastructural morphometry of the pancreatic β-cell. Diabetologia 9: 115–119.
de Velasco, B., T. Erclik, D. Shy, J. Sclafani, H. Lipshitz *et al.*, 2007 Specification and development of the pars intercerebralis and pars lateralis, neuroendocrine command centers in the Drosophila brain. Dev. Biol. 302: 309–323.
Dietzl, G., D. Chen, F. Schnorrer, K. C. Su, Y. Barinova *et al.*, 2007 A genome-wide transgenic RNAi library for conditional gene inactivation in Drosophila. Nature 448: 151–156.
Donelan, M. J., G. Morfini, R. Julyan, S. Sommers, L. Hays *et al.*, 2002 Ca2+-dependent dephosphorylation of kinesin heavy chain on beta-granules in pancreatic beta-cells. Implications for regulated beta-granule transport and insulin exocytosis. J. Biol. Chem. 277: 24232–24242.
Dong, H., M. Kumar, Y. Zhang, A. Gyulkhandanyan, Y. Y. Xiang *et al.*, 2006 Gamma-aminobutyric acid up- and downregulates insulin secretion from beta cells in concert with changes in glucose concentration. Diabetologia 49: 697–705.
Escurat, M., K. Djabali, C. Huc, F. Landon, C. Becourt *et al.*, 1991 Origin of the beta cells of the islets of Langerhans is further questioned by the expression of neuronal intermediate filament proteins, peripherin and NF-L, in the rat insulinoma RIN5F cell line. Dev. Neurosci. 13: 424–432.
Fujita, P. A., B. Rhead, A. S. Zweig, A. S. Hinrichs, D. Karolchik *et al.*, 2011 The UCSC Genome Browser database: update 2011. Nucleic Acids Res. 39: D876–D882.
Geminard, C., E. J. Rulifson, and P. Leopold, 2009 Remote control of insulin secretion by fat cells in Drosophila. Cell Metab. 10: 199–207.
German, M. S., 1993 Glucose sensing in pancreatic islet beta cells: the key role of glucokinase and the glycolytic intermediates. Proc. Natl. Acad. Sci. USA 90: 1781–1785.
Glassmeier, G., M. Hopfner, E. O. Riecken, B. Mann, H. Buhr *et al.*, 1998 Inhibition of L-type calcium channels by somatostatins in human neuroendocrine tumor cells of the gut. Ann. N. Y. Acad. Sci. 859: 208–209.
Goodwin, P. R., J. M. Sasaki,, and P. Juo, 2012 Cyclin-dependent kinase 5 regulates the polarized trafficking of neuropeptide-containing dense-core vesicles in Caenorhabditis elegans motor neurons. J. Neurosci. 32: 8158–8172.
Gronke, S., D. F. Clarke, S. Broughton, T. D. Andrews, and L. Partridge, 2010 Molecular evolution and functional characterization of Drosophila insulin-like peptides. PLoS Genet. 6: e1000857.
Harashima, S., A. Clark, M. R. Christie, and A. L. Notkins, 2005 The dense core transmembrane vesicle protein IA-2 is a regulator of vesicle number and insulin secretion. Proc. Natl. Acad. Sci. USA 102: 8704–8709.
Haselton, A. T., and Y. W. Fridell, 2010 Adult Drosophila melanogaster as a model for the study of glucose homeostasis. Aging (Albany, NY) 2: 523–526.
Hickey, A. J., J. W. Bradley, G. L. Skea, M. J. Middleditch, C. M. Buchanan *et al.*, 2009 Proteins associated with immunopurified granules from a model pancreatic islet beta-cell system: proteomic snapshot of an endocrine secretory granule. J. Proteome Res. 8: 178–186.
Hoy, M., P. O. Berggren, and J. Gromada, 2003 Involvement of protein kinase C-epsilon in inositol hexakisphosphate-induced exocytosis in mouse pancreatic beta-cells. J. Biol. Chem. 278: 35168–35171.
Huang da, W., B. T. Sherman, and R. A. Lempicki, 2009a Bioinformatics enrichment tools: paths toward the comprehensive functional analysis of large gene lists. Nucleic Acids Res. 37: 1–13.
Huang da, W., B. T. Sherman, and R. A. Lempicki, 2009b Systematic and integrative analysis of large gene lists using DAVID bioinformatics resources. Nat. Protoc. 4: 44–57.
Hwang, H. J., and E. Rulifson, 2011 Serial specification of diverse neuroblast identities from a neurogenic placode by Notch and Egfr signaling. Development 138: 2883–2893.
Hwangbo, D. S., B. Gershman, M. P. Tu, M. Palmer, and M. Tatar, 2004 Drosophila dFOXO controls lifespan and regulates insulin signalling in brain and fat body. Nature 429: 562–566.
Ikeya, T., M. Galic, P. Belawat, K. Nairz, and E. Hafen, 2002 Nutrient-dependent expression of insulin-like peptides from neuroendocrine cells in the CNS contributes to growth regulation in Drosophila. Curr. Biol. 12: 1293–1300.
Iser, W. B., M. S. Gami, and C. A. Wolkow, 2007 Insulin signaling in Caenorhabditis elegans regulates both endocrine-like and cell-autonomous outputs. Dev. Biol. 303: 434–447.
Iyer, E. P., and D. N. Cox, 2010 Laser capture microdissection of Drosophila peripheral neurons. J. Vis. Exp.
Iyer, E. P., S. C. Iyer, M. J. Sulkowski, and D. N. Cox, 2009 Isolation and purification of Drosophila peripheral neurons by magnetic bead sorting. J. Vis. Exp., No. 34: pii: 1599.
Jensen, J., 2004 Gene regulatory factors in pancreatic development. Dev. Dyn. 229: 176–200.
Karolchik, D., R. Baertsch, M. Diekhans, T. S. Furey, A. Hinrichs *et al.*, 2003 The UCSC Genome Browser Database. Nucleic Acids Res. 31: 51–54.
Kasai, H., H. Hatakeyama, M. Ohno, and N. Takahashi, 2010 Exocytosis in islet beta-cells. Adv. Exp. Med. Biol. 654: 305–338.
Kasai, K., M. Ohara-Imaizumi, N. Takahashi, S. Mizutani, S. Zhao *et al.*, 2005 Rab27a mediates the tight docking of insulin granules onto the plasma membrane during glucose stimulation. J. Clin. Invest. 115: 388–396.
Kern, J. V., Y. V. Zhang, S. Kramer, J. E. Brenman, and T. M. Rasse, 2013 The kinesin-3, unc-104 regulates dendrite morphogenesis and synaptic development in *Drosophila*. Genetics 195: 59–72.

Kieffer, T. J., R. S. Heller, C. A. Leech, G. G. Holz, and J. F. Habener, 1997 Leptin suppression of insulin secretion by the activation of ATP-sensitive K+ channels in pancreatic beta-cells. Diabetes 46: 1087–1093.

Kim, J., H. Bang, S. Ko, I. Jung, H. Hong *et al.*, 2008 Drosophila ia2 modulates secretion of insulin-like peptide. Comp. Biochem. Physiol. A Mol. Integr. Physiol. 151: 180–184.

Kim, S. K., and E. J. Rulifson, 2004 Conserved mechanisms of glucose sensing and regulation by Drosophila corpora cardiaca cells. Nature 431: 316–320.

Kimura, T., and I. Niki, 2011 Rab27a in pancreatic beta-cells, a busy protein in membrane trafficking. Prog. Biophys. Mol. Biol. 107: 219–223.

Kimura, T., Y. Kaneko, S. Yamada, H. Ishihara, T. Senda *et al.*, 2008 The GDP-dependent Rab27a effector coronin 3 controls endocytosis of secretory membrane in insulin-secreting cell lines. J. Cell Sci. 121: 3092–3098.

Ku, G. M., H. Kim, I. W. Vaughn, M. J. Hangauer, C. M. Oh *et al.*, 2012 Research resource: RNA-Seq reveals unique features of the pancreatic β-cell transcriptome. Mol. Endocrinol. 26: 1783–1792.

Lam, T. K., R. Gutierrez-Juarez, A. Pocai, and L. Rossetti, 2005 Regulation of blood glucose by hypothalamic pyruvate metabolism. Science 309: 943–947.

Lang, J. E., M. J. Magbanua, J. H. Scott, G. M. Makrigiorgos, G. Wang *et al.*, 2009 A comparison of RNA amplification techniques at sub-nanogram input concentration. BMC Genomics 10: 326.

Li, W., S. G. Kennedy, and G. Ruvkun, 2003 daf-28 encodes a C. elegans insulin superfamily member that is regulated by environmental cues and acts in the DAF-2 signaling pathway. Genes Dev. 17: 844–858.

Lilly, B., B. Zhao, G. Ranganayakulu, B. M. Paterson, R. A. Schulz *et al.*, 1995 Requirement of MADS domain transcription factor D-MEF2 for muscle formation in Drosophila. Science 267: 688–693.

Lo, K. Y., A. Kuzmin, S. M. Unger, J. D. Petersen, and M. A. Silverman, 2011 KIF1A is the primary anterograde motor protein required for the axonal transport of dense-core vesicles in cultured hippocampal neurons. Neurosci. Lett. 491: 168–173.

Mendez, C. F., I. B. Leibiger, B. Leibiger, M. Hoy, J. Gromada *et al.*, 2003 Rapid association of protein kinase C-epsilon with insulin granules is essential for insulin exocytosis. J. Biol. Chem. 278: 44753–44757.

Meng, Y. X., G. W. Wilson, M. C. Avery, C. H. Varden, and R. Balczon, 1997 Suppression of the expression of a pancreatic beta-cell form of the kinesin heavy chain by antisense oligonucleotides inhibits insulin secretion from primary cultures of mouse beta-cells. Endocrinology 138: 1979–1987.

Miguel-Aliaga, I., S. Thor, and A. P. Gould, 2008 Postmitotic specification of Drosophila insulinergic neurons from pioneer neurons. PLoS Biol. 6: e58.

Miller, M. R., K. J. Robinson, M. D. Cleary, and C. Q. Doe, 2009 TU-tagging: cell type-specific RNA isolation from intact complex tissues. Nat. Methods 6: 439–441.

Nassel, D. R., 2012 Insulin-producing cells and their regulation in physiology and behavior of Drosophila. Can. J. Zool. 90: 476–488.

Newsholme, P., C. Gaudel, and N. H. McClenaghan, 2010 Nutrient regulation of insulin secretion and beta-cell functional integrity. Adv. Exp. Med. Biol. 654: 91–114.

Ni, J. Q., M. Markstein, R. Binari, B. Pfeiffer, L. P. Liu *et al.*, 2008 Vector and parameters for targeted transgenic RNA interference in Drosophila melanogaster. Nat. Methods 5: 49–51.

O'Brien, L. E., S. S. Soliman, X. Li, and D. Bilder, 2011 Altered modes of stem cell division drive adaptive intestinal growth. Cell 147: 603–614.

Okada, Y., H. Yamazaki, Y. Sekine-Aizawa, and N. Hirokawa, 1995 The neuron-specific kinesin superfamily protein KIF1A is a unique monomeric motor for anterograde axonal transport of synaptic vesicle precursors. Cell 81: 769–780.

Okamoto, N., N. Yamanaka, Y. Yagi, Y. Nishida, H. Kataoka *et al.*, 2009 A fat body-derived IGF-like peptide regulates postfeeding growth in Drosophila. Dev. Cell 17: 885–891.

Pack-Chung, E., P. T. Kurshan, D. K. Dickman, and T. L. Schwarz, 2007 A Drosophila kinesin required for synaptic bouton formation and synaptic vesicle transport. Nat. Neurosci. 10: 980–989.

Park, D., J. A. Veenstra, J. H. Park,, and P. H. Taghert, 2008 Mapping peptidergic cells in Drosophila: where DIMM fits in. PLoS ONE 3: e1896.

Philipson, L. H., A. Kusnetsov, T. Larson, Y. Zeng, and G. Westermark, 1993 Human, rodent, and canine pancreatic beta-cells express a sodium channel alpha 1-subunit related to a fetal brain isoform. Diabetes 42: 1372–1377.

Puig, O., M. T. Marr, M. L. Ruhf, and R. Tjian, 2003 Control of cell number by Drosophila FOXO: downstream and feedback regulation of the insulin receptor pathway. Genes Dev. 17: 2006–2020.

Rajan, A., and N. Perrimon, 2012 Drosophila cytokine unpaired 2 regulates physiological homeostasis by remotely controlling insulin secretion. Cell 151: 123–137.

Rao, S., C. Lang, E. S. Levitan, and D. L. Deitcher, 2001 Visualization of neuropeptide expression, transport, and exocytosis in Drosophila melanogaster. J. Neurobiol. 49: 159–172.

Rayburn, L. Y., J. Rhea, S. R. Jocoy, and M. Bender, 2009 The proprotein convertase amontillado (amon) is required during Drosophila pupal development. Dev. Biol. 333: 48–56.

Rolls, M. M., 2011 Neuronal polarity in Drosophila: sorting out axons and dendrites. Dev. Neurobiol. 71: 419–429.

Rorsman, P., and E. Renstrom, 2003 Insulin granule dynamics in pancreatic beta cells. Diabetologia 46: 1029–1045.

Rulifson, E. J., S. K. Kim, and R. Nusse, 2002 Ablation of insulin-producing neurons in flies: growth and diabetic phenotypes. Science 296: 1118–1120.

Satoh, A., F. Tokunaga, S. Kawamura, and K. Ozaki, 1997 In situ inhibition of vesicle transport and protein processing in the dominant negative Rab1 mutant of Drosophila. J. Cell Sci. 110 (Pt 23): 2943–2953.

Settle, S. H. Jr., M. M. Green, and K. C. Burtis, 1995 The silver gene of Drosophila melanogaster encodes multiple carboxypeptidases similar to mammalian prohormone-processing enzymes. Proc. Natl. Acad. Sci. USA 92: 9470–9474.

Siekhaus, D. E., and R. S. Fuller, 1999 A role for amontillado, the Drosophila homolog of the neuropeptide precursor processing protease PC2, in triggering hatching behavior. J. Neurosci. 19: 6942–6954.

Sivachenko, A., Y. Li, K. C. Abruzzi, and M. Rosbash, 2013 The transcription factor Mef2 links the Drosophila core clock to Fas2, neuronal morphology, and circadian behavior. Neuron 79: 281–292.

Slaidina, M., R. Delanoue, S. Gronke, L. Partridge, and P. Leopold, 2009 A Drosophila insulin-like peptide promotes growth during nonfeeding states. Dev. Cell 17: 874–884.

Sousa-Nunes, R., L. L. Yee, and A. P. Gould, 2011 Fat cells reactivate quiescent neuroblasts via TOR and glial insulin relays in Drosophila. Nature 471: 508–512.

Spletter, M. L., J. Liu, H. Su, E. Giniger, T. Komiyama *et al.*, 2007 Lola regulates Drosophila olfactory projection neuron identity and targeting specificity. Neural Dev. 2: 14.

Stenmark, H., 2009 Rab GTPases as coordinators of vesicle traffic. Nat. Rev. Mol. Cell Biol. 10: 513–525.

Tabei, S. M., S. Burov, H. Y. Kim, A. Kuznetsov, T. Huynh *et al.*, 2013 Intracellular transport of insulin granules is a subordinated random walk. Proc. Natl. Acad. Sci. USA 110: 4911–4916.

Takahashi, N., H. Hatakeyama, H. Okado, A. Miwa, T. Kishimoto *et al.*, 2004 Sequential exocytosis of insulin granules is associated with redistribution of SNAP25. J. Cell Biol. 165: 255–262.

Tatar, M., 2004 The neuroendocrine regulation of Drosophila aging. Exp. Gerontol. 39: 1745–1750.

Tirouvanziam, R., C. J. Davidson, J. S. Lipsick, and L. A. Herzenberg, 2004 Fluorescence-activated cell sorting (FACS) of Drosophila hemocytes reveals important functional similarities to mammalian leukocytes. Proc. Natl. Acad. Sci. USA 101: 2912–2917.

Trapnell, C., L. Pachter, and S. L. Salzberg, 2009 TopHat: discovering splice junctions with RNA-Seq. Bioinformatics 25: 1105–1111.

Trapnell, C., B. A. Williams, G. Pertea, A. Mortazavi, G. Kwan *et al.*, 2010 Transcript assembly and quantification by RNA-Seq reveals unannotated transcripts and isoform switching during cell differentiation. Nat. Biotechnol. 28: 511–515.

Uno, T., K. Sakamoto, Y. Isoyama, S. Hiragaki, Y. Uno *et al.*, 2013 Relationship between the expression of Rab family GTPases and neuropeptide hormones in the brain of Bombyx mori. Histochem. Cell Biol. 139: 299–308.

Van Gelder, R. N., M. E. von Zastrow, A. Yool, W. C. Dement, J. D. Barchas *et al.*, 1990 Amplified RNA synthesized from limited quantities of heterogeneous cDNA. Proc. Natl. Acad. Sci. USA 87: 1663–1667.

Wang, E., 2005 RNA amplification for successful gene profiling analysis. J. Transl. Med. 3: 28.

Wang, E., L. D. Miller, G. A. Ohnmacht, E. T. Liu, and F. M. Marincola, 2000 High-fidelity mRNA amplification for gene profiling. Nat. Biotechnol. 18: 457–459.

Wang, H., R. Ishizaki, J. Xu, K. Kasai, E. Kobayashi *et al.*, 2013 The Rab27a effector exophilin7 promotes fusion of secretory granules that have not been docked to the plasma membrane. Mol. Biol. Cell 24: 319–330.

Wang, M. C., D. Bohmann, and H. Jasper, 2005 JNK extends life span and limits growth by antagonizing cellular and organism-wide responses to insulin signaling. Cell 121: 115–125.

Wang, S., N. Tulina, D. L. Carlin, and E. J. Rulifson, 2007 The origin of islet-like cells in Drosophila identifies parallels to the vertebrate endocrine axis. Proc. Natl. Acad. Sci. USA 104: 19873–19878.

Xu, E., M. Kumar, Y. Zhang, W. Ju, T. Obata *et al.*, 2006 Intra-islet insulin suppresses glucagon release via GABA-GABAA receptor system. Cell Metab. 3: 47–58.

Ye, B., Y. Zhang, W. Song, S. H. Younger, L. Y. Jan *et al.*, 2007 Growing dendrites and axons differ in their reliance on the secretory pathway. Cell 130: 717–729.

Yi, Z., H. Yokota, S. Torii, T. Aoki, M. Hosaka *et al.*, 2002 The Rab27a/granuphilin complex regulates the exocytosis of insulin-containing dense-core granules. Mol. Cell. Biol. 22: 1858–1867.

Yonekawa, Y., A. Harada, Y. Okada, T. Funakoshi, Y. Kanai *et al.*, 1998 Defect in synaptic vesicle precursor transport and neuronal cell death in KIF1A motor protein-deficient mice. J. Cell Biol. 141: 431–441.

Zahn, T. R., J. K. Angleson, M. A. MacMorris, E. Domke, J. F. Hutton *et al.*, 2004 Dense core vesicle dynamics in Caenorhabditis elegans neurons and the role of kinesin UNC-104. Traffic 5: 544–559.

Zhang, H., J. Liu, C. R. Li, B. Momen, R. A. Kohanski *et al.*, 2009 Deletion of Drosophila insulin-like peptides causes growth defects and metabolic abnormalities. Proc. Natl. Acad. Sci. USA 106: 19617–19622.

Zhang, J., K. L. Schulze, P. R. Hiesinger, K. Suyama, S. Wang *et al.*, 2007 Thirty-one flavors of Drosophila rab proteins. Genetics 176: 1307–1322.

Communicating editor: N. Perrimon

GENETICS

Supporting Information
http://www.genetics.org/lookup/suppl/doi:10.1534/genetics.113.160663/-/DC1

Insight into Insulin Secretion from Transcriptome and Genetic Analysis of Insulin-Producing Cells of *Drosophila*

Jian Cao, Julie Ni, Wenxiu Ma, Vanessa Shiu, Luis A. Milla, Sangbin Park, Maria L. Spletter, Sheng Tang, Jun Zhang, Xing Wei, Seung K. Kim, and Matthew P. Scott

DOI: 10.1534/genetics.113.160663

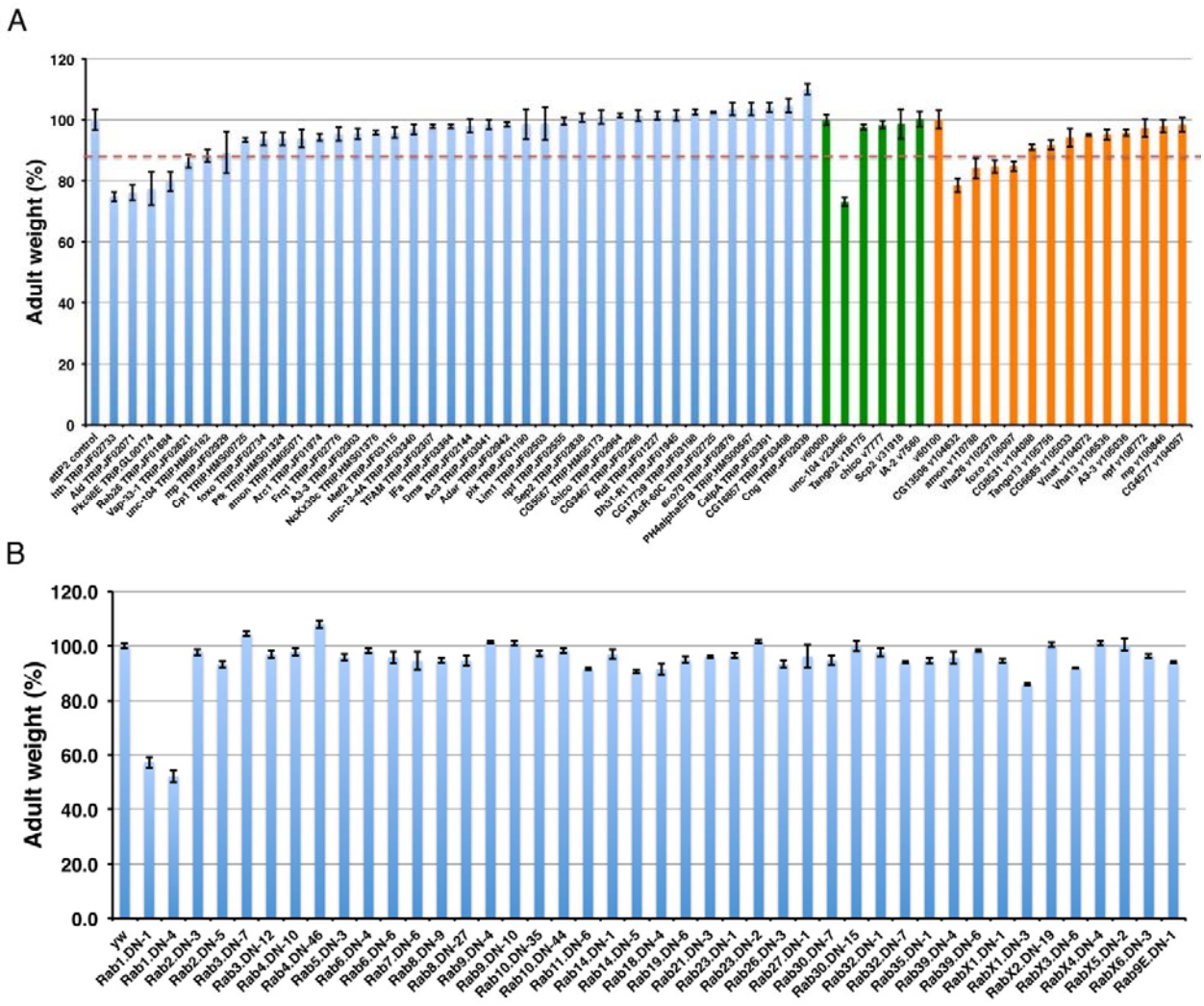

Figure S1 RNAi screen of IPC-enriched genes and Rab-DNs for growth phenotypes. (A) 56 *UAS-RNAi* lines covering 50 genes were crossed to *Ilp2-Gal4* and the progeny male adults were examined for their weights. These genes represent a wide range of molecular functions. They encode signaling molecules, transcription factors, neuropeptide receptors, motor proteins, sugar metabolic enzymes, synapse organizers, and etc. RNAi lines from different RNAi libraries are color-coded. Blue: Harvard TRiP lines; Green: VDRC GD lines; Orange: VDRC KK lines. The red-dashed line indicates the 90% adult weight cutoff. Error bars represent S.E.M. **(B)** 43 *UAS-Rab-DNs* lines covering 29 Rabs were crossed to *Ilp2-Gal4* and the progeny male adults were examined for their weight. Error bars represent S.E.M.

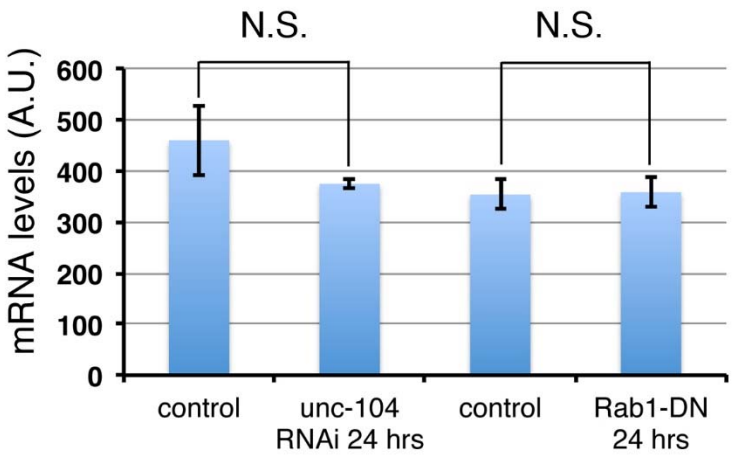

Figure S2 Measurement of larval brain *Ilp2* transcript levels when *unc-104* mRNA was depleted or Rab1 protein function was inhibited. *Ilp2* transcript levels were compared by quantitative RT-PCR between control and *unc-104* knockdown in IPCs for 24 hrs (*tubGal80^{ts}*, *Ilp2>unc-104 RNAi*), or Rab1 inhibition in IPCs for 24 hrs (*tubGal80^{ts}*, *Ilp2>Rab1-DN*). *Rpl32* was used as an internal control. N.S.: non significant. Error bars represent S.E.M.

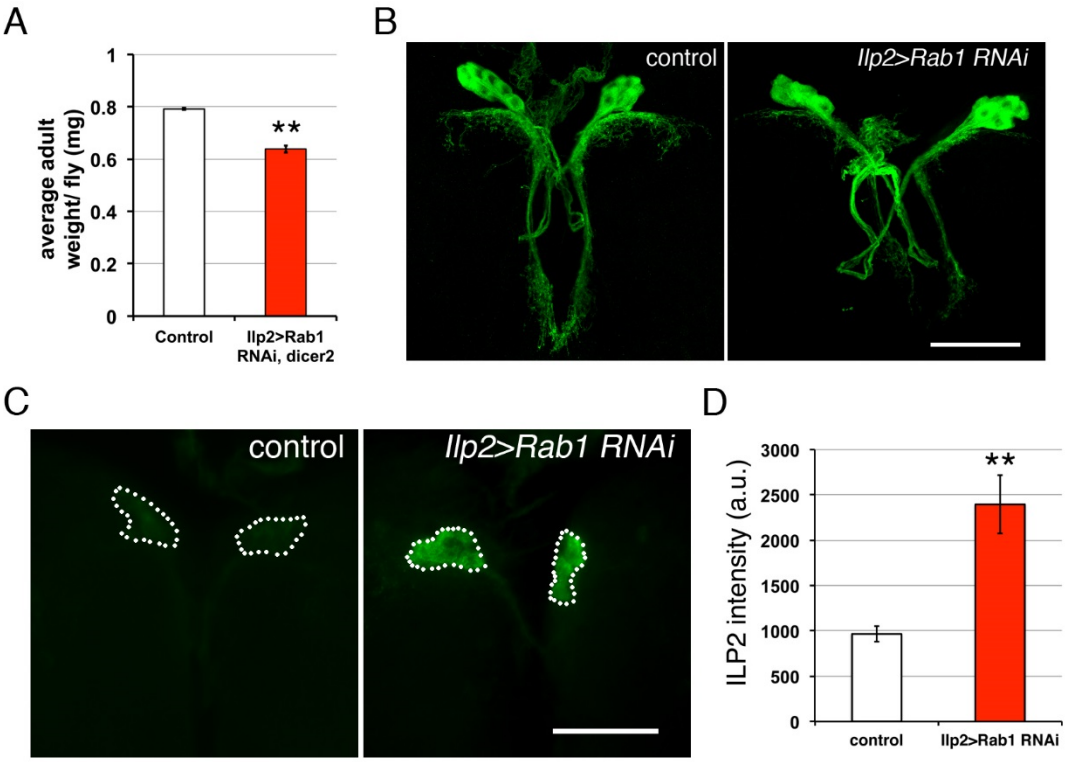

Figure S3 Expressing Rab1 RNAi in IPCs results in accumulation of ILP2 in IPCs. (A) Adult weights were compared between control flies (*Ilp2-Gal4>attP2 control*, n = 63 flies) and flies expressing *Rab1 RNAi* in IPCs (*Ilp2>Rab1 RNAi*, *dicer2*; n = 60 flies). **(B)** IPC neurite structure was labeled with *Ilp2>mCD8-GFP* in *Ilp2>Rab1 RNAi*, *dicer2* and control (*Ilp2>dicer2*, *attP2 control*) brains. **(C-D)** ILP2 fluorescence intensities in the brain IPC cell bodies were compared between control (n = 8 brains) and *Rab1 RNAi* expressed in IPCs (n = 8 brains). Scale bars: 50µm. Error bar: S.E.M. **p<0.01.

Files S1-S4

Available for download as .mov files at http://www.genetics.org/lookup/suppl/doi:10.1534/genetics.113.160663/-/DC1

File S1 Movie of IPCs at different developmental stages. Green: *Ilp2>mCD8-GFP*; Red: *Ilp2>nuclear-RFP*; blue: DAPI.

File S2 Rotating view of larval IPCs at 93 hrs after embryo deposition. Green: *Ilp2>mCD8-GFP*; Red: *Ilp2>nuclear-RFP*.

File S3 Rotating view of pupal IPCs at 146 hrs after embryo deposition. Green: *Ilp2>mCD8-GFP*; Red: *Ilp2>nuclear-RFP*.

File S4 Rotating view of adult IPCs at 239 hrs after embryo deposition. Green: *Ilp2>mCD8-GFP*; Red: *Ilp2>nuclear-RFP.*

File S5

Supplemental Materials and Methods

Detailed protocol for sequencing library construction

1) 400ng of amplified mRNA was fragmented to 10-200nt using 10x RNA fragmentation buffer (Ambion) and was purified using regular ethanol precipitation method with 0.35µl of GlycoBlue (Ambion). 2) 3' end the RNA samples were dephosphorylated using 10x Antarctic Phosphatase Buffer and 0.5 µl Antarctic Phosphatase (NEB) at 37 °C for 20 minutes. The reaction was heat inactivated at 75°C for 10 minutes. 3) 5' end of RNA samples was phosphorylated using 10x T4 DNA ligase buffer (it has 1mM ATP final) and T4 PNK (NEB) at 37 °C for 30 minutes. The RNAs in the reactions were purified using ammonium acetate and ethanol precipitation with 2µl of GlycoBlue (Ambion). 4) The RNA samples are then ligated to 3' linker (5'-/5rApp/CTG TAG GCA CCA TCA AT/3ddC/-3') (synthesized by IDT) using T4 RNA ligase 1 (NEB), 5X ATP-free T4 RNA ligase buffer (16.5 mM DTT, 41.5% glycerol, 250 mM HEPES-KOH, pH8.3, 50 mM $MgCl_2$, 50 µg/ml acetylated BSA), and 10% DMSO at 37 °C for one hour. The RNAs in the reactions were purified using ammonium acetate and ethanol precipitation with 2µl of GlycoBlue (Ambion). The RNA samples were then run on 6% TBE-Urea PAGE Gel (Invitrogen). The 100-200nt bands were cut and elute overnight with 400µl stop solution (1M ammonium acetate and 10mM EDTA) at 4°C overnight. The RNAs in the supernatant was purified using regular ethanol precipitation method with 2µl of GlycoBlue (Ambion). 5) The RNA samples are ligated to 5' linker (with bar code) using T4 RNA ligase 1 (NEB), 10x T4 RNA ligase 1 buffer (NEB), and 10% DMSO at 37°C for 1 hour. The RNAs was purified by ammonium acetate and ethanol precipitation and gel purification as described in step 4. The 5' barcoded linkers are synthesized by IDT. IPC1: 5'-/5AmMC6/ ACG CTC TTC CGA TCT rCrUrGrG-3', IPC2: 5'-/5AmMC6/ ACG CTC TTC CGA TCT rCrGrUrC-3', Control 1: 5'-/5AmMC6/ ACG CTC TTC CGA TCT rArCrUrU-3', Control 2: 5'-/5AmMC6/ ACG CTC TTC CGA TCT rCrCrCrU-3'. 6) cDNA of the RNA samples were reverse transcribed using SuperScript III (Invitrogen) following manufacture's protocol. The primer sequence used for reverse transcription is 5'-ATT GAT GGT GCC TAC AG-3'. 7) The cDNA samples were amplified using Taq (NEB) following manufacture's protocol. Forward primer: 5'-GAT ACG GCG ACC ACC GAG ATC TAC ACT CTT TCC CTA CAC GAC GCT CTT CCG ATC T-3'. Reverse primer: 5'-CAA GCA GAA GAC GGC ATA CGA GCT CTT CCG ATC TAT TGA TGG TGC CTA CAG-3'. The PCR products (200-300nt) were purified using Qiagen PCR purification kit. The purified PCR samples were diluted to 10nM and were sequenced using Illumina GA II sequencing system.

Table S1 Number of aligned mRNA reads to the *D. melanogaster* Refseq mRNA.

Samples	Barcode	Total # of post-filter reads	Mapped to dm3 genome and transcriptome
Control	ACTT	1,077,110	239,757
	TCGC	3,175,833	398,659
IPC	CTGG	3,118,626	592,440
	CGTC	3,833,784	417,340

Tables S2-S5

Available for download as Excel files at http://www.genetics.org/lookup/suppl/doi:10.1534/genetics.113.160663/-/DC1

Table S2 List of all genes with aligned reads in laser-captured IPC and control samples.

Table S3 List of 193 IPC-enriched genes with their annotated molecular functions.

Table S4 Full list of biological functional clusters annotated by DAVID with IPC-enriched transcripts.

Table S5 List of 109 IPC-enriched genes and their mouse orthologs. The mouse orthologs that have higher expression levels in beta cells compared to other non-beta cell tissues (Ku et al.) are indicated.

Table S6 *Drosophila* stocks used in this study.

yw	*UAS YFP.Rab2 DN-5*	*UAS YFP.Rab23 DN-2*
w^{1118}	*UAS YFP.Rab3 DN-7*	*UAS YFP.Rab26 DN-3*
Ilp2-Gal4/Cy (Eric Rulifson)	*UAS YFP.Rab3 DN-12*	*UAS YFP.Rab27 DN-1*
UAS-GFP-myc-2xFYVE (Bloomington)	*UAS YFP.Rab4 DN-10*	*UAS YFP.Rab30 DN-7*
UAS-Grasp65-GFP (Bloomington)	*UAS YFP.Rab 4 DN-46*	*UAS YFP.Rab30 DN-15*
UAS-mCD8-GFP (Liqun Luo)	*UAS YFP.Rab5 DN-3*	*UAS YFP.Rab32 DN-1*
UAS-mtdTomato (Liqun Luo)	*UAS YFP.Rab6 DN-4*	*UAS YFP.Rab32 DN-7*
UAS- nuclear-RFP (Liqun Luo)	*UAS YFP.Rab6 DN-6*	*UAS YFP.Rab35 DN-1*
UAS-Tau-LacZ (Bloomington)	*UAS YFP.Rab7 DN-6*	*UAS YFP.Rab39 DN-4*
UAS-Khc::nod-LacZ (Bloomington)	*UAS YFP.Rab8 DN-9*	*UAS YFP.Rab39 DN-6*
UAS-dicer2 (VDRC)	*UAS YFP.Rab8 DN-27*	*UAS YFP.RabX1 DN-1*
yv; attP2, y+ (control for TRiP RNAi lines, Bloomington)	*UAS YFP.Rab9 DN-4*	*UAS YFP.RabX1 DN-3*
UAS-lamin-GFP (Bloomington)	*UAS YFP.Rab9 DN-10*	*UAS YFP.RabX2 DN-19*
Rab1-Gal4 (Robin Hiesinger)	*UAS YFP.Rab10 DN-35*	*UAS YFP.RabX3 DN-6*
Ilp2-Gal4 (Ping Shen)	*UAS YFP.Rab10 DN-44*	*UAS YFP.RabX4 DN-4*
UAS-unc-104-GFP (Bill Saxton)	*UAS YFP.Rab11 DN-6*	*UAS YFP.RabX5 DN-2*
UAS-unc-104-mCherry-HA (Tom Schwarz)	*UAS YFP.Rab14 DN-1*	*UAS YFP.RabX6 DN-3*
UAS-ANF-GFP (Bill Saxton)	*UAS YFP.Rab14 DN-5*	*UAS YFP.Rab9E DN-1*
Elav-Gal4 (Bloomington)	*UAS YFP.Rab18 DN-4*	*UAS YFP.Rab1 WT-1*
UAS YFP.Rab1 DN-1	*UAS YFP.Rab19 DN-6*	*VDRC RNAi* lines
UAS YFP.Rab1 DN-4	*UAS YFP.Rab21 DN-3*	*TRiP RNAi* lines
UAS YFP.Rab2 DN-3	*UAS YFP.Rab23 DN-1*	$tub\text{-}Gal80^{ts}$ (Bloomington)